Importance of Human-Induced Nitrogen Flux Increases for Simulated Arctic Warming

Hyung-Gyu Lim,[a,b] Jong-Yeon Park,[c] John P. Dunne,[d] Charles A. Stock,[d] Sung-Ho Kang,[e] and Jong-Seong Kug[b]

[a] *Princeton University/Atmospheric and Oceanic Sciences Program, Princeton, New Jersey*
[b] *Division of Environmental Science and Engineering, POSTECH, Pohang, South Korea*
[c] *Department of Earth and Environmental Sciences, Jeonbuk National University, Jeollabuk-do, South Korea*
[d] *National Oceanic and Atmospheric Administration/Geophysical Fluid Dynamics Laboratory, Princeton, New Jersey*
[e] *Korea Polar Research Institute, Incheon, South Korea*

ABSTRACT: Human activities such as fossil fuel combustion, land-use change, nitrogen (N) fertilizer use, emission of livestock, and waste excretion accelerate the transformation of reactive N and its impact on the marine environment. This study elucidates that anthropogenic N fluxes (ANFs) from atmospheric and river deposition exacerbate Arctic warming and sea ice loss via physical–biological feedback. The impact of physical–biological feedback is quantified through a suite of experiments using a coupled climate–ocean–biogeochemical model (GFDL-CM2.1-TOPAZ) by prescribing the preindustrial and contemporary amounts of riverine and atmospheric N fluxes into the Arctic Ocean. The experiment forced by ANFs represents the increase in ocean N inventory and chlorophyll concentrations in present and projected future Arctic Ocean relative to the experiment forced by preindustrial N flux inputs. The enhanced chlorophyll concentrations by ANFs reinforce shortwave attenuation in the upper ocean, generating additional warming in the Arctic Ocean. The strongest responses are simulated in the Eurasian shelf seas (Kara, Barents, and Laptev Seas; 65°–90°N, 20°–160°E) due to increased N fluxes, where the annual mean surface temperature increase by 12% and the annual mean sea ice concentration decrease by 17% relative to the future projection, forced by preindustrial N inputs.

KEYWORDS: Arctic; Climate change; Ocean models

1. Introduction

Human activities, such as fossil fuel combustion, land-use change, nitrogen (N) fertilizer use, emission of livestock, and waste excretion, increase the N in the atmosphere and land (Boyer et al. 2006; Galloway et al. 2008). Anthropogenic N widely spreads to freshwater and marine ecosystems via atmospheric deposition and river delivery (Green et al. 2004; Boyer et al. 2006; Gruber and Galloway 2008). The anthropogenic N cascades the coastal and freshwater eutrophication (Galloway et al. 2003), hypoxia (Diaz and Rosenberg 2008), and harmful algal blooms (Anderson et al. 2002).

While the magnitude of anthropogenic N fluxes (ANFs) and the mechanism by which they affect the marine ecosystem and consequent results in climate warming are still unclear (Galloway et al. 2004; Green et al. 2004; Gruber and Galloway 2008; Holmes et al. 2012; Regnier et al. 2013; McClelland et al. 2016), there has been a consensus of increasing N fluxes in the Arctic Ocean. For example, Green et al. (2004) reported global estimates of preindustrial and contemporary fluxes of N, which are estimated to be doubled from rivers from $1.3 \, \text{Tg yr}^{-1}$ in preindustrial to $2.64 \, \text{Tg yr}^{-1}$ in the contemporary period in the Arctic Ocean, and estimated to be fourfold from the atmospheric deposition from $0.61 \, \text{Tg yr}^{-1}$ in preindustrial to $2.11 \, \text{Tg yr}^{-1}$ in the contemporary period in the Arctic Ocean.

ANF fluxes are indispensable components of the Arctic Ocean because of N limitation in the marine ecosystem (Tremblay and Gagnon 2009; Popova et al. 2012; Tremblay et al.

2015). The influence of river runoff on the Arctic Ocean is stronger than the global ocean in terms of volume per input of Arctic river runoff about 10% of the global river runoff while the small volume about 1% of the Arctic Ocean in the global ocean (Jakobsson 2002). It has been reported that river runoff has been increased 7% through the six largest Eurasian rivers in the Arctic Ocean from 1936 to 1999 (McClelland et al. 2004) and expected to even further increase in the future due to Arctic moistening (Peterson et al. 2002; Min et al. 2008). In addition, sources of atmospheric N deposition in the European region have been widespread remotely from land to the air and to be precipitated in the N-limited Arctic Ocean far from the Arctic coast (Galloway et al. 2004, 2008). Under this condition, the increase in such remote forcing from the riverine nutrient flux and atmospheric deposition can increase the phytoplankton primary production in the N-limited Arctic Ocean (Pabi et al. 2008; Arrigo and van Dijken 2011; Tank et al. 2012; Le Fouest et al. 2013; Arrigo and van Dijken 2015; Le Fouest et al. 2015; Tremblay et al. 2015; Terhaar et al. 2019). For example, Terhaar et al. (2019, 2021) recently suggested that riverine nutrient and coastal erosion fuels 28%–51% of the current net primary production and doubled riverine nutrient become increased future primary production by 11% in the pan-Arctic Ocean.

Changing phytoplankton pigments (i.e., chlorophyll concentration) alters the ocean's optical properties, such as its shortwave attenuation by changing the inherent absorption and by scattering shortwave radiation (Morel 1988; Morel and Antoine 1994; Manizza et al. 2005). An increase in shortwave radiation will result in an increase of the upper-ocean temperature as shown by fully coupled climate models that account

for marine chlorophyll (Marzeion et al. 2005; Anderson et al. 2009; Lengaigne et al. 2009; Park et al. 2015; Lim et al. 2019b; Séférian et al. 2019). In particular, Lengaigne et al. (2009) used the Institut Pierre Simone Laplace IPSL-CM4 model to suggest feedback between phytoplankton chlorophyll and Arctic warming: additional shortwave absorption by chlorophyll ($1.3 \, \mathrm{mg \, m^{-3}}$) in a fully coupled experiment increases the surface ocean heat ~15% and decreases the sea ice volume ~17% more than in a constant chlorophyll ($0.06 \, \mathrm{mg \, m^{-3}}$) experiment. Following this, Park et al. (2015) used projections from the Geophysical Fluid Dynamics Laboratory GFDL-CM2.1-TOPAZ (Tracers of Ocean Phytoplankton with Allometric Zooplankton) model and the Max Planck Earth system model (MPI-ESM) to further suggest that increased spring chlorophyll under greenhouse warming can reduce Arctic sea ice and amplify projected Arctic warming. Lim et al. (2019b) stated that increased spring mean chlorophyll and decreased summer interannual chlorophyll variability may amplify Arctic surface warming through nonlinear rectifications of chlorophyll variability. However, none of the existing Arctic chlorophyll feedback studies considers the changes in the background fluxes of N via rivers and atmospheric deposition whereas models have considered the changes in marine N cycle, horizontal, and vertical ocean circulation due to climate change.

The present study quantifies the impact of increased background fluxes of allochthonous N on the Arctic sea ice and surface air temperature in the future climate using GFDL-CM2.1-TOPAZ with prescribed N external preindustrial and contemporary forcing of the river and atmospheric depositions. Section 2 provides a detailed description of the model experimental design. Section 3 presents increased nitrate and chlorophyll responses in the experiment forced by anthropogenic N fluxes than by preindustrial N fluxes in the future climate, highlighting the spatial and seasonal dependencies of these responses and the mechanistic link between enhanced N and enhanced chlorophyll. Section 4 shows the additional ocean surface heating caused by an increase in chlorophyll in the experiment forced by anthropogenic N fluxes than by preindustrial N fluxes in the future climate. Section 5 quantifies the impact of increased N fluxes on the future climate in the Arctic. Last, section 6 presents the summary and discussion.

2. Model experiment

a. GFDL-CM2.1-TOPAZ

In this study, we employed GFDL-CM2.1-TOPAZ, a fully coupled climate ocean–biogeochemical model. GFDL-CM2.1-TOPAZ consists of an atmospheric model (AM2), land model (LM2), modular ocean model (MOM5), sea ice simulator (SIS), and an ocean biogeochemistry model (BGC), namely Tracers of Phytoplankton with Allometric Zooplankton version 2 (TOPAZ2) (Dunne et al. 2012b, 2013).

The horizontal resolution of AM2 is 2° in latitude × 2.5° in longitude on a regular grid and 24 vertical levels in a hybrid coordinate system. The dynamical core of AM2 uses the finite volume method (Anderson et al. 2004; Lin 2004). The horizontal resolution of LM2 is the same as that of AM2 and

includes soil sensible and latent heat storage, groundwater storage, stomatal resistance, and a rudimentary runoff-routing scheme for river delivery to the ocean (Milly and Shmakin 2002; Anderson et al. 2004). A constant sea salt concentration is prescribed throughout the well-mixed marine boundary layer (Delworth et al. 2006). The horizontal resolution of MOM5 (Griffies 2012) is 1° in latitude between 30° and 65° longitude, and it telescopes to 1/3° toward the equatorial region; the polar region is nonuniform, and the horizontal grid switches from spherical to bipolar poleward above 65°N (mean = $2831 \, \mathrm{km^2}$, maximum = $5129 \, \mathrm{km^2}$, minimum = $46 \, \mathrm{km^2}$) for treating polar singularity over the ocean (Murray 1996). SIS has full ice dynamics, a three-layer framework, five different ice thickness categories, and the same tripolar grid (bipolar in Northern Hemisphere over land and the South Pole) as that on the open ocean (Murray 1996; Winton 2000). TOPAZ2 considers 30 tracers to describe the cycles of carbon: two inorganic N (nitrate NO_3 and ammonium NH_4) and two organic N (labile and semilabile dissolved organic nitrogen), one inorganic phosphorus (PO_4) and one organic phosphorus (semilabile dissolved organic phosphorus), silicon, iron, oxygen, alkalinity, and lithogenic material as well as pelagic calcite, aragonite, and surface sediment calcite dynamics. TOPAZ2 includes the water column denitrification under suboxia, and sediment denitrification after Middelburg et al. (1996). Diazotrophs represent facultative nitrogen fixers with nitrogen fixation inhibited by nitrate (NO_3), ammonia (NH_4), and oxygen (O_2) (Dunne et al. 2013). Following Geider et al. (1997), TOPAZ2 considers three explicit phytoplankton groups whose growth depends on light, temperature, and nutrients.

TOPAZ1 can capture various observed biogeochemical patterns across ocean biomes (Dunne et al. 2013), leading to its relatively good performance in simulating global chlorophyll ($r = 0.72$, bias = $0.04 \, \mathrm{mgChl \, m^{-3}}$) and global integrated net primary production ($r = 0.69$, bias = $6.8 \, \mathrm{mol \, C \, m^{-2} \, yr^{-1}}$) (Laufkötter et al. 2015) and the seasonal skills of the CO_2 flux and the net primary production in the Northern Hemisphere above 49°–90°N (Anav et al. 2013) among models from phase 5 of the Coupled Model Intercomparison Project (CMIP5). TOPAZ2 well simulates the depth-averaged nitrate concentration patterns in the Arctic ($r = 0.66$) but yields a low concentration bias of $-3.8 \, \mathrm{mmol \, m^{-3}}$ compared with in situ observation (Lee et al. 2016); nonetheless, a more thorough comparison is needed due to the low observation data coverage in the entire Arctic basin (Vancoppenolle et al. 2013). The present set of control simulations in GFDL-CM2.1-TOPAZ captures the double peaks of the chlorophyll seasonal cycle over ice-free areas of the pan-Arctic region; the first peak in May and later the second peak in October compared with European Space Agency Ocean Color Climate Change Initiative project version 3 (ESA-CCI-v3) satellite-derived chlorophyll observation (Müller et al. 2015) in the open ocean of pan-Arctic (Lim et al. 2019a).

b. Manizza shortwave heating scheme

MOM5 uses the shortwave heating scheme of Manizza et al. (2005). This scheme is based on the light attenuation coefficient of two bands as a function of chlorophyll concentration

(Morel 1988). It further considers the influence of chlorophyll concentration on light attenuation and chlorophyll's self-shading effect that accomplishes by reducing the light input to below-ocean depth. The light attenuation follows the *e*-folding depth of the Lambert–Beer law, but the attenuation coefficients in this scheme are subsequently modulated by the chlorophyll concentration in the horizontal and vertical grids at every integration time. The Manizza shortwave heating scheme, therefore, interplays 1) the modulation of the shortwave attenuation in the ocean by the vertically resolved chlorophyll concentration prognostics simulated by TOPAZ2 (Griffies 2012), 2) its impact on heat energy redistribution in the ocean depth, and 3) its impact on ocean dynamics and the atmosphere; such interplay facilitates the air–sea–biological interaction in GFDL-CM2.1-TOPAZ. The configuration of the Manizza shortwave heating scheme is consistent with those in previous chlorophyll–shortwave feedback studies that used GFDL-CM2.1-TOPAZ (Lim et al. 2018, 2019a,b).

c. Initialization and spinup

First, the ocean-only model (MOM-SIS-TOPAZ) was spun up 300 years as a cold start forced by Coordinated Ocean-Ice Reference Experiments (CORE) (Large and Yeager 2004) for an ocean and sea ice model developed by the National Center for Atmospheric Research (NCAR) with climatological air temperature, humidity, radiation, precipitation, and winds; *World Ocean Atlas 2005* observations for nitrate, phosphate, silicate, and oxygen (Antonov et al. 2006; Garcia et al. 2006a,b; Locarnini et al. 2006); Global Ocean Data Analysis Project data (Key et al. 2004) for alkalinity and preindustrial dissolved inorganic carbon; initial sediment calcite derived from bottom water conditions and fluxes (Dunne et al. 2012a); and lithogenic dust and soluble iron (Fan et al. 2006). With the initial conditions of MOM-SIS-TOPAZ, GFDL-CM2.1-TOPAZ was subsequently integrated for a 500-yr spinup (total spinup time is 800 years). The concentrations of greenhouse gases CO_2, CH_4, and N_2O were fixed at 1990 levels. This spinup of 800 years was prescribed by external forcing of preindustrial N inputs: 1) preindustrial amounts of monthly-mean-based climatological forcing of atmospheric wet and dry N depositions ($0.02 \, gN \, yr^{-1}$ averaged over the pan-Arctic region) simulated by a global three-dimensional chemical transport model called Model of Ozone and Related Chemical Tracers (MOZART) (Horowitz et al. 2003) and 2) annual mean–based climatological forcing of riverine N ($0.093 \, gN \, m^{-3}$ averaged in the pan-Arctic) simulated by the constituent transport model (CTM) (Green et al. 2004). The 800-yr spinup of GFDL-CM2.1-TOPAZ is the same structure reported in Lim et al. (2018, 2019a,b). The remaining long-term spinup drift in GFDL-CM2.1-TOPAZ was stabilized for 550–800 years for averaged pan-Arctic chlorophyll ($5.1 \times 10^{-4} \, mg \, m^{-3} decade^{-1}$) and nitrate ($1.3 \times 10^{-2} \, \mu mol \, kg^{-1} \, decade^{-1}$) concentrations up to 30 m mean and sea ice concentration (SIC) ($-0.1\% \, decade^{-1}$).

d. Experimental design

With the initial condition of 800-yr spinup, as implemented in section 2c, two baseline experiments, namely preindustrial N (N_{pi}-1xCO_2) and contemporary N (N_{1990}-1xCO_2), were further

implemented in the present study using different sets of preindustrial and contemporary amounts of N external forcing of riverine N and atmospheric N deposition (Table 1).

The river delivery of N was obtained from CTM (Green et al. 2004) for GFDL-CM2.1-TOPAZ spinup and control as the external forcing of N. This river N dataset is an annual mean–based estimate and one of the few global estimates available for climate models of preindustrial and contemporary river N delivery amounts in aquatic systems. However, there has been uncertainty in terms of no seasonality of this riverine N forcing in the Arctic Ocean, which might be overestimated in winter and underestimated in summer, and in the global riverine loading, as the estimate of $35 \, Tg \, yr^{-1}$ using CTM (Green et al. 2004) is considerably lower than the $54 \, Tg \, yr^{-1}$ estimated by van Drecht et al. (2001) based on point and nonpoint sources of N; also, the estimate of $2.64 \, Tg \, yr^{-1}$ in the Arctic Ocean using CTM is larger than $1.26 \, Tg \, yr^{-1}$ estimated by Holmes et al. (2012); additionally, we do not account for the coastal erosion (Fritz et al. 2017). Such differences must be considered carefully in interpretations of the present results and existences of uncertainties. We used the estimates of Green et al. (2004) in the present study that the riverine N concentration of this dataset in the pan-Arctic Ocean is approximately $0.093 \, gN \, m^{-3}$ in preindustrial (Fig. 1a) to $0.122 \, gN \, m^{-3}$ in contemporary (Fig. 1b), reflecting an increase of about 30.3% (Fig. 1c).

The atmospheric deposition of monthly N was obtained from a model simulation by the Chemistry-Climate Model Initiative (CCMI) through the joint International Global Atmospheric Chemistry (IGAC) and Stratosphere–Troposphere Processes and Their Role in Climate (SPARC) CCMI (https://blogs.reading.ac.uk/ccmi/forcing-databases-in-support-of-cmip6/) for GFDL-CM2.1-TOPAZ control as another external forcing of N. The CCMI atmospheric N deposition forcing (Hegglin et al. 2016) was generated using a state-of-the-art chemistry–climate model (NCAR CAM-chem; Lamarque et al. 2012) and was recommended officially by CMIP6 to force Earth system models that lack atmospheric N deposition interactions (Jones et al. 2016). In the pan-Arctic region, the atmospheric N deposition is estimated to be $0.019 \, gN \, m^{-2} \, yr^{-1}$ in preindustrial (Fig. 1d), which is similar to that of MOZART, and approximately $0.049 \, gN \, m^{-2} \, yr^{-1}$ in contemporary (Fig. 1e), reflecting an increase of about 156.6% (Fig. 1f). The increase in the Arctic Ocean is stronger in the Atlantic sector near the European continent than that in the Pacific sector near the East Siberian and Chukchi Seas; the spatial distribution is consistent with the other atmospheric N deposition estimates (Horowitz et al. 2003; Galloway et al. 2004; Krishnamurthy et al. 2007).

The N_{pi}-1xCO_2 run was forced by the preindustrial global river N and the preindustrial global atmospheric N deposition with constant values in greenhouse gas concentrations at 1990 levels. The N_{1990}-1xCO_2 run was forced by contemporary global river N and contemporary global atmospheric N deposition with constant values in greenhouse gas concentrations at 1990 levels (353 ppm). Thus, the difference between these experiments (N_{1990}-1xCO_2 − N_{pi}-1xCO_2) gives the effects of increases in N caused by human influence in the present-day climate. Both idealized experiments were integrated for an

TABLE 1. Summary of four experiments used in this study. All experiments feature different sets of atmospheric CO_2 concentrations and N fluxes into the ocean surface, as prescribed by simulated N forcing obtained from Green et al. (2004) and CCMI for CMIP6. The other anthropogenic forcing (CH_4 and N_2O) is fixed at the year 1990 values across all experiments.

Expt	Riverine N (Green et al. 2004)	Atmospheric N deposition (CCMI for CMIP6)	Atmospheric CO_2	Simulated period
N_{pi}-1xCO_2	Preindustrial	1850	1990	500 years
N_{1990}-1xCO_2	Mid-1990s	1990	1990	500 years
N_{pi}-2xCO_2	Preindustrial	1850	1% increase from 1990 until doubled	110 years, 10-member ensemble
N_{1990}-2xCO_2	Mid-1990s	1990	1% increase from 1990 until doubled	110 years, 10-member ensemble

additional 500 years (i.e., total 1300-yr spinup) to minimize the long-term drift due to changes in N forcing sets. After 200 years, in the pan-Arctic, surface chlorophyll (-7.77×10^{-2} mg m^{-3} decade^{-1} in N_{pi}-1xCO_2 and 7.53×10^{-2} mg m^{-3} decade^{-1} in N_{1990}-1xCO_2), surface nitrate (-1.96×10^{-3} μmol m^{-3} decade^{-1} in N_{pi}-1xCO_2 and

6.84×10^{-3} μmol m^{-3} decade^{-1} in N_{1990}-1xCO_2), and sea ice (2.03×10^{-3}% decade^{-1} in N_{pi}-1xCO_2 and -9.74×10^{-2}% decade^{-1} in N_{1990}-1xCO_2) concentrations were stabilized from the year 1000 to the year 1300; thus, the last 300 years of both N_{pi}-1xCO_2 and N_{1990}-1xCO_2 experiments were taken into account
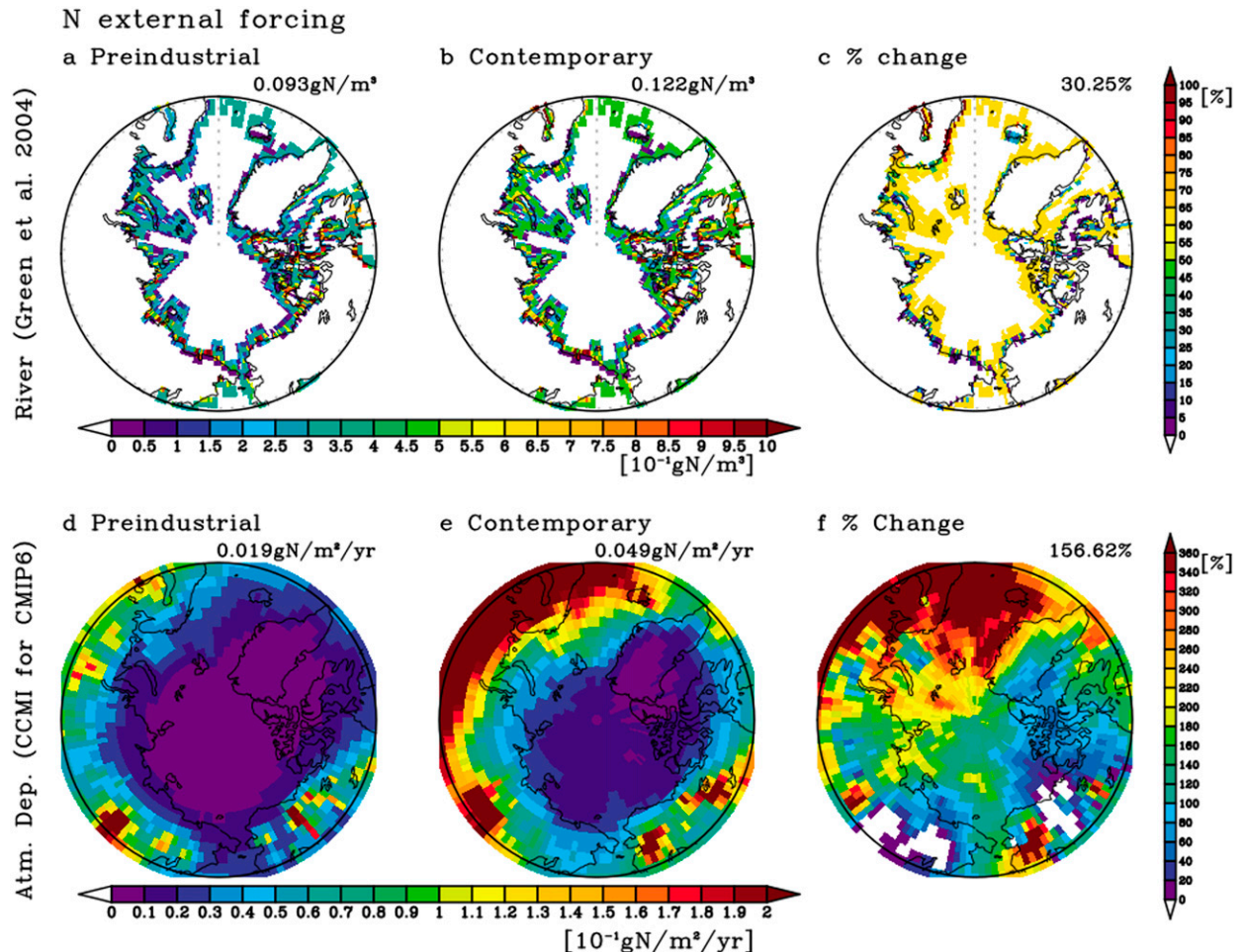

FIG. 1. External forcing N used in present study: (left) preindustrial, (center) contemporary, and (right) percentage change between preindustrial and contemporary amounts through (top) river and (bottom) atmospheric depositions and their quantities averaged for the pan-Arctic (top-right value in each panel).
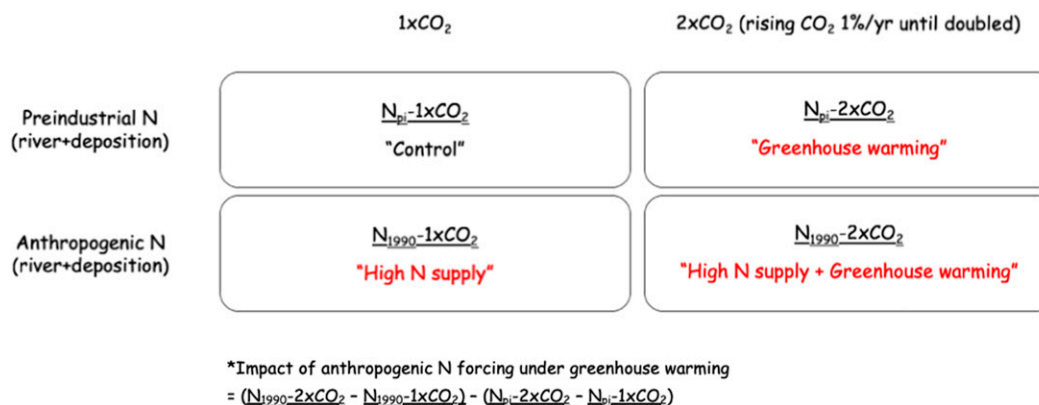
FIG. 2. Schematic figure of experimental design.

for the analysis of the present-day climate. We checked the vertically integrated meridional nitrate transport to 500 m calculated by climatology averaged across the years 1980–2000 of *World Ocean Atlas 2013* (*WOA13*) data (Garcia et al. 2014) and Simple Ocean Data Assimilation (SODA) version 2.2.4 data (Giese and Ray 2011). The observational nitrate transport is about 8.23 (2.09) $mmol\,kg^{-1}\,cm\,s^{-1}$ in the Atlantic (Pacific) sector. The simulated nitrate transport in the Atlantic (Pacific) sector is around 9.19 (1.41) $mmol\,kg^{-1}\,cm\,s^{-1}$ in N_{pi}-$1xCO_2$, which has increased to 10.28 (1.45) $mmol\,kg^{-1}\,cm\,s^{-1}$ in N_{1990}-$1xCO_2$ in the Atlantic (Pacific) sector.

To consider the joint effects of anthropogenic N forcing and transient twenty-first-century warming, we conducted additional idealized experiments that incorporated transient warming for the future climate. For these experiments, the initial conditions (the year 1990) were taken from N_{pi}-$1xCO_2$ and N_{1990}-$1xCO_2$. CO_2 concentrations were increased by 1% per year until they doubled in 2060 (706 ppm). Then, CO_2 was fixed until 2100 (other greenhouse gases were fixed as constant values at 1990 levels). The N external forcing for these experiments was fixed at preindustrial (N_{pi}-$2xCO_2$) and contemporary (N_{1990}-$2xCO_2$) levels of atmospheric N deposition and river N, respectively. For both $2xCO_2$ experiments, an ensemble of 10 projections was constructed by initiating members from a 10-yr interval after the spinup of N_{pi}-$1xCO_2$ and N_{1990}-$1xCO_2$.

In summary, four experiment types were conducted: one with preindustrial N in present-day climate (N_{pi}-$1xCO_2$), one with anthropogenic N in present-day climate (N_{1990}-$1xCO_2$), one 10-member ensemble with preindustrial N and transient warming (N_{pi}-$2xCO_2$), and one 10-member ensemble with both anthropogenic N and transient warming (N_{1990}-$2xCO_2$). This stepwise experiment was conducted to consider the effect of not only increased CO_2 but also increased N, as represented in Fig. 2.

e. Summary of experimental design

Based on the experimental design as described in section 2d, we conducted riverine N fluxes and atmospheric N deposition from preindustrial and contemporary amounts on the present-day climate with fixed CO_2 and the future climate with doubled CO_2 (Table 1). The two experiments represent the response in the present-day climate fixed by $1xCO_2$ and forced by riverine N fluxes and atmospheric N deposition in different amounts of the preindustrial period (N_{pi}-$1xCO_2$) and the contemporary period (N_{1990}-$1xCO_2$); those results are described in section 3a. These two experiments are utilized in the other two experiments as initial conditions in the future climate projection increased by 1% of CO_2 until doubled with 10 ensembles (i.e., N_{pi}-$2xCO_2$ and N_{1990}-$2xCO_2$), with amounts of riverine N fluxes and atmospheric N deposition from the same preindustrial period with N_{pi}-$1xCO_2$ and contemporary period with N_{1990}-$1xCO_2$; those results are described in section 3b. Based on these four experiments (Fig. 2), we quantify the impact of ANF by calculating the differences among all experimental sets: "impact of ANF" = (N_{1990}-$2xCO_2$ − N_{1990}-$1xCO_2$) − (N_{pi}-$2xCO_2$ − N_{pi}-$1xCO_2$), those results are described in section 4 and section 5. For $2xCO_2$ runs, we analyzed responses in the last 30 years of both N_{1990}-$2xCO_2$ and N_{pi}-$2xCO_2$ experiments (i.e., 2071–2100 at the saturated state of the doubled atmospheric CO_2 relative to 1990 levels).

3. Marine biogeochemical response against increased background N fluxes

a. Present-day climate

The annual mean nitrate and chlorophyll concentrations in the Arctic Ocean (>65°N) are increased about 19% (from 2.95 $\mu mol\,kg^{-1}$ in N_{pi}-$1xCO_2$ to 3.52 in N_{1990}-$1xCO_2$) and 6.2% (from 0.38 $mg\,m^{-3}$ N_{pi}-$1xCO_2$ to 0.40 in N_{1990}-$1xCO_2$), respectively. These annual mean nitrate and chlorophyll concentrations in N_{1990}-$1xCO_2$ are closer to the observations than those in N_{pi}-$1xCO_2$ in the pan-Arctic Ocean (Table 2). The annual mean nitrate concentration is underestimated in N_{pi}-$1xCO_2$ by about −0.52 $\mu mol\,kg^{-1}$ and −0.29 in the pan-Arctic Ocean relative to the *WOA13* (Garcia et al. 2014) and mapped climatology data of the Global Ocean Data Analysis Project version 2 (GLODAPv2) (Lauvset et al. 2016) observations, which is similar to that in a previous report (Lee et al. 2016). The chlorophyll is also underestimated about −0.3 $mg\,m^{-3}$ in N_{pi}-$1xCO_2$ relative to ESA-CCI-v3 (Müller et al. 2015), which

TABLE 2. Annual mean sea surface temperature (SST), sea ice concentration (SIC), and sea ice extent (SIE >15% of SIC) and nitrate and chlorophyll concentrations up to 30 m depth in the pan-Arctic Ocean in N_{pi}-1xCO_2 and N_{1990}-1xCO_2 experiments and biases in apparencies compared to 1980–2000 climatology in HadISST (Rayner et al. 2003), *World Ocean Atlas 2013* (*WOA13*) data (Garcia et al. 2014), mapped climatology data of the Global Ocean Data Analysis Project version 2 (GLODAPv2; Lauvset et al. 2016), and 1998–2004 climatology data in the European Space Agency Ocean Color Climate Change Initiative project version 3 (Müller et al. 2015). The chlorophyll values are averaged over ice-free conditions [<15% of SIC in HadISST (Rayner et al. 2003) and <15% of SIC in experiments].

	N_{pi}-1xCO_2	N_{1990}-1xCO_2	WOA13, GLODAPv2	ESA-CCI-v3	HadISST
SIC (%)	56.1 (−11.8)	56.2 (−11.8)			67.9
SIE (millions of km^2)	8.34 (+0.62)	8.35 (+0.63)			7.72
Nitrate (μmol kg^{-1})	2.95 (−0.52, −0.29)	3.51 (+0.04, +0.27)	3.47, 3.24		
Chlorophyll (mg m^{-3})	0.35 (−0.3)	0.37 (−0.28)		0.65	

can be partly caused by the lower nitrate concentration in N_{pi}-1xCO_2 relative to observations. In the pan-Arctic Ocean, the nitrate concentration in the N_{1990}-1xCO_2 forced with contemporary amounts of N fluxes is much closer to the observation than that forced with preindustrial N fluxes but is slightly overestimated by approximately +0.04 to +0.27 μmol kg^{-1}. Specifically, the regional nitrate concentrations in N_{pi}-1xCO_2, which are underestimated over the Kara, Laptev, and East Siberian Seas, are increased by 15%–19% in N_{1990}-1xCO_2, which are much closer to the observation; the overestimated nitrate concentration in the Barents Sea of N_{1990}-1xCO_2 causes the nitrate concentration bias of N_{1990}-1xCO_2 in the pan-Arctic Ocean (Table 3). The annual mean chlorophyll concentration bias is −0.28 mg m^{-3}, which slightly corrects around 7% of the bias in N_{pi}-1xCO_2 (Table 2).

A spatial map of the nitrate and chlorophyll concentration differences in the present-day climate between the two baseline experiments of the preindustrial N fluxes (N_{pi}-1xCO_2) and contemporary N fluxes (N_{1990}-1xCO_2) is shown in Fig. 3. The forced anthropogenic N enhances the annual mean chlorophyll concentration over the pan-Arctic Ocean (Fig. 3d) in a manner consistent with the annual nitrate concentration increases associated with larger ANFs (Fig. 3a). The annual mean nitrate and chlorophyll concentrations in the Arctic Ocean (>65°N) are increased by about 19% (from 2.95 to 3.52 μmol kg^{-1}) and 6.2% (from 0.38 to 0.40 mg m^{-3}), respectively. However, the magnitude of the chlorophyll increase is distinctively stronger in summer [June to August (JJA)] (~11%) than in spring [March to May (MAM)] (~1%; Figs. 3e,f); the increased nitrate concentration patterns, in contrast, are consistent throughout the seasons (Figs. 3b,c).

The seasonal cycle and percentage change in nitrate and chlorophyll concentrations are shown in Fig. 4. The seasonal cycle of nitrate in N_{1990}-1xCO_2 shows an increase throughout

all seasons, specifically a stronger difference of nitrate concentration between N_{pi}-1xCO_2 and N_{1990}-1xCO_2 from winter to spring than in summer (Fig. 4a). The percentage change in nitrate in summer is stronger than that in nitrate in the other seasons due to the ocean stratification in summer and following a minimum of nitrate seasonal cycle. While the absolute quantity of changes in nitrate in N_{1990}-1xCO_2 is stronger in spring, the chlorophyll response is strongly represented from June to September (Fig. 4b). A comparison of the changes in chlorophyll with changes in the nitrate ratio shows that smaller changes in summer nitrate enhance chlorophyll more effectively than do large changes in spring (Fig. 4c). GFDL-CM2.1-TOPAZ simulates the seasonal dependency of chlorophyll against colimiting factors, such as light and nutrients, as shown in Lim et al. (2019a). The anthropogenic N forcing associated with the nitrate concentration anomaly induces a positive chlorophyll anomaly in the summer chlorophyll concentration; this pattern is consistent with the N limitation during stratified, low–sea ice summer conditions. Meanwhile, the nitrate and chlorophyll anomalies are not correlated in spring, given that light exerts a more dominant control on spring chlorophyll than does N.

b. Future climate

As shown in the above section, forced anthropogenic N contributes to increases in nitrate concentration in the present-day climate. Modeling studies indicate that the differential forcing of background fluxes of allochthonous N into the Arctic Ocean may affect the N limitation strength under Arctic warming (Cabré et al. 2015; Lim et al. 2019b). For all experiments (preindustrial and contemporary), the changing climate reduces the aquatic N concentration and sea ice cover in the Arctic during spring and summer (Figs. 5a,b,d,e). Increased CO_2 and the resulting greenhouse warming (hereafter greenhouse warming) melt of sea ice. Consequently, there is less

TABLE 3. Annual mean nitrate concentration (μmol kg^{-1}) up to 30 m depth in the regional Arctic Ocean: Barents (70°–80°N, 30°–70°E), Kara (70°–80°N, 70°–100°E), Laptev (70°–80°N, 100°–150°E), and East Siberian (70°–80°N, 160°E–180°) Seas in N_{pi}-1xCO_2 and N_{1990}-1xCO_2 experiments with *World Ocean Atlas 2013* (Garcia et al. 2014) and GLODAPv2 (Lauvset et al. 2016) data.

	N_{pi}-1xCO_2	N_{1990}-1xCO_2	WOA13	GLODAPv2
Barents Sea	4.68	5.58 (+19.2%)	3.33	2.55
Kara Sea	1.82	2.16 (+18.7%)	3.28	2.63
Laptev Sea	1.62	1.87 (+15.4%)	2.62	2.96
East Siberian Sea	1.83	2.17 (+18.5%)	2.31	1.97

Nitrate ($N_{1990}-1xCO_2 - N_{pi}-1xCO_2$)
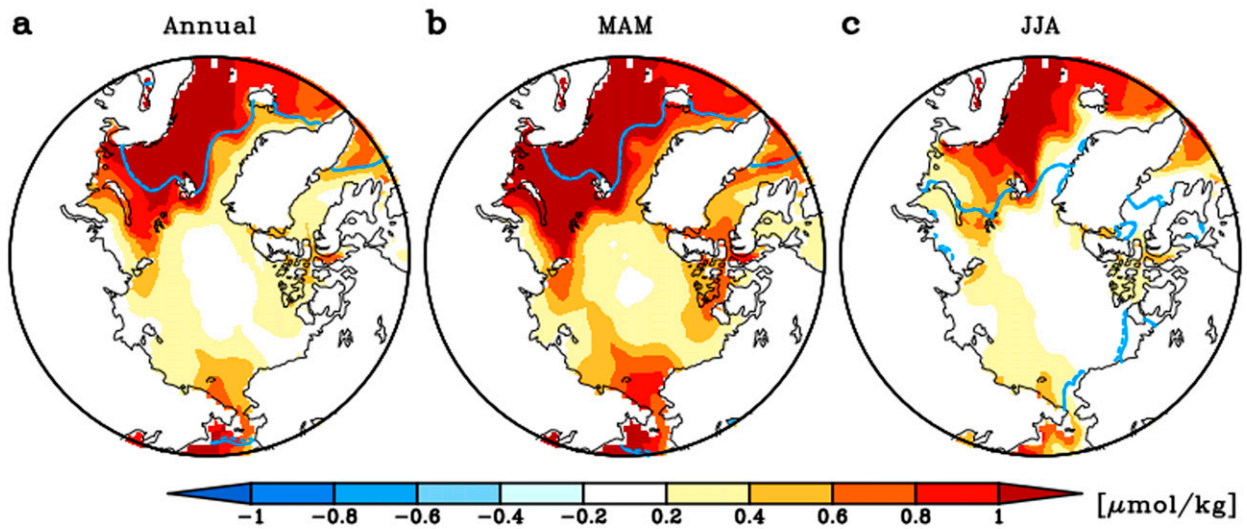
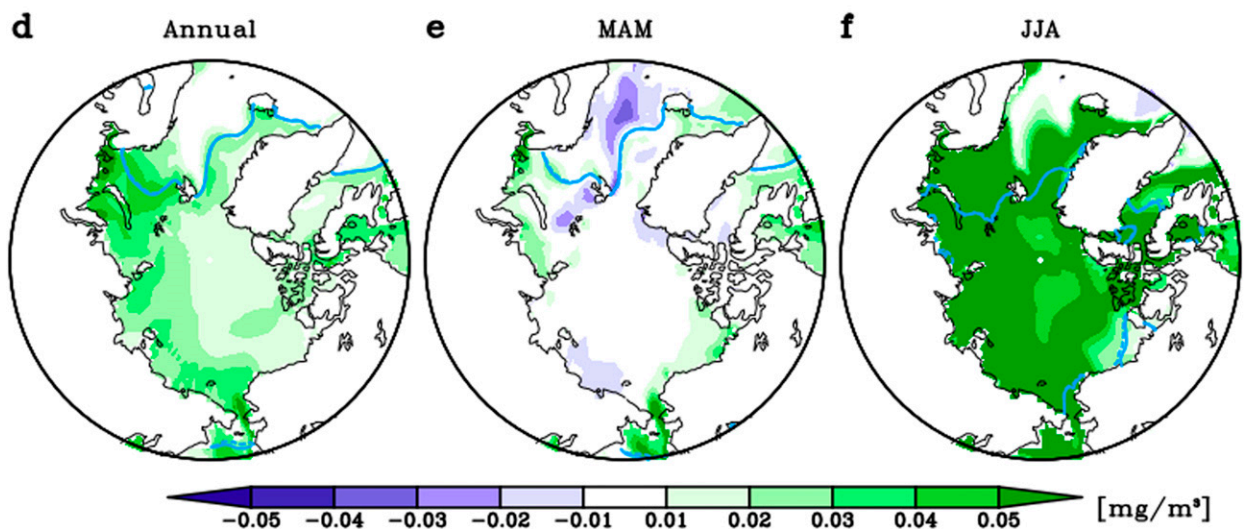
Chlorophyll ($N_{1990}-1xCO_2 - N_{pi}-1xCO_2$)

FIG. 3. Nitrate difference between N_{pi}-1xCO_2 and N_{1990}-1xCO_2 averaged for (a) annual mean, (b) spring mean (MAM), and (c) summer (JJA) up to 30 m ocean depth. (d)–(f) As in (a)–(c), but for a difference in the chlorophyll concentration. The contour lines denote the sea ice edge below 15% of the concentration of N_{pi}-1xCO_2 (solid) and N_{1990}-1xCO_2 (dashed).

shortwave reflection; thus, more shortwave radiation can enhance stratification due to surface warming and freshwater flux in most seasons. The climatological nitrate (both the maximum in April and the minimum in August) is reduced under greenhouse warming, as shown in Table 4.

The impact of ANF, as defined in section 2e, on nitrate concentration under greenhouse warming is computed as the difference between the impact of warming on experiments with preindustrial N and the impact of warming on experiments with anthropogenic N (Figs. 5c,f). This formulation of ANF ensures that the impact of warming on preindustrial N is separated from the desired anthropogenic impacts. The nitrate concentration response to Arctic warming is increased by ANF by approximately 6.5% in spring (from $-0.93\,\mu\text{mol}\,\text{kg}^{-1}$ preindustrial N flux to $-0.87\,\mu\text{mol}\,\text{kg}^{-1}$ contemporary N flux) (Fig. 5c). This response is the strongest in the Kara–Barents–Laptev Seas (herein called Eurasian shelf seas) due to the spatial distribution of the atmospheric N deposition, and the increase is stronger near the European region than the Pacific sector (Fig. 1f). The difference in nitrate is about 9.8% in the
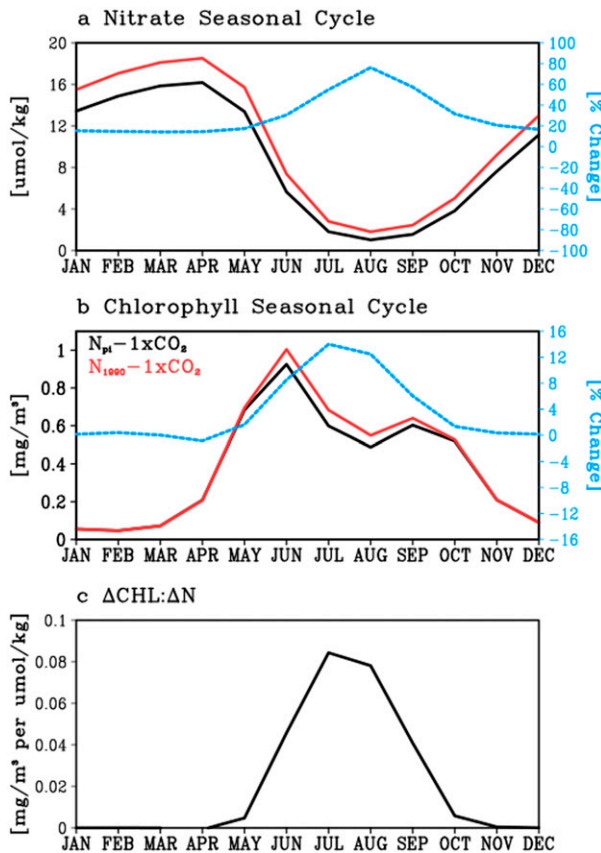
FIG. 4. Seasonal cycle of (a) nitrate and (b) chlorophyll concentrations (left axis) and its percentage changes (blue dashed; right axis) from N_{pi}-1xCO_2 (black line) to N_{1990}-1xCO_2 (red line). (c) The Δchlorophyll to Δnitrate ratio averaged for the pan-Arctic ($\Delta = N_{1990}$-1x$CO_2 - N_{pi}$-1xCO_2).

maximum in April from $-0.87\,\mu$mol kg^{-1} preindustrial N flux to $-0.78\,\mu$mol kg^{-1} contemporary N flux (Table 4), suggesting an offset in the reduced surface nitrate. The slower nitrate decrease via the increased N fluxes alters the nitrate inventory in the future climate, which will fertilize the chlorophyll concentration anomaly in the anthropogenic-N-forced set (N_{1990}-2x$CO_2 - N_{1990}$-1xCO_2) more than that in the preindustrial-N-forced set (N_{pi}-2x$CO_2 - N_{1990}$-1xCO_2).

The stoichiometric ratio of nitrate relative to phosphate (N:P), nutrient uptake, and release by phytoplankton is approximately similar to the Redfield et al. (1963) N:P ratio of 16, which can be modulated by human-induced N fluxes into the marine environment (Gruber and Sarmiento 1997; Kim et al. 2014). The N:P ratio is simply calculated here as $N^* = [NO_3^-] - 16 \times [PO_4^{3-}]$. Regarding the present-day climate in the pan-Arctic Ocean, N^* is negative in both experiments, which implies a nitrate-limited condition (contour in Figs. 6a,b,d,e). As increased N fluxes replenish nitrates, the simulated N^* of N_{1990}-1xCO_2 is slightly higher than that of N_{pi}-1xCO_2 but is still negative.

In the future climate, N^* increases in spring and summer regardless of whether N fluxes are smaller or larger (shading in Figs. 6a,b,d,e). Despite having a fixed amount of contemporary

N flux, allochthonous N has a higher probability of reaching the Arctic in the future than the present-day because of the expansion of the open-ocean area. However, ANFs intensify the magnitude of the positive N^* anomaly relative to the N^* changes in the preindustrial N fluxes in both spring and summer under greenhouse warming (Figs. 6c,f). The impact of ANF on N^* is the strongest in the Eurasian shelf seas. This is consistent with previous findings suggesting that the Eurasian shelf seas have the largest source of ANF (Fig. 1).

The chlorophyll concentration changes between the future (2xCO_2) and present-day (1xCO_2) climate runs under preindustrial N fluxes (N_{pi}-2x$CO_2 - N_{pi}$-1xCO_2; Figs. 7a,d) and contemporary N fluxes (N_{1990}-2x$CO_2 - N_{1990}$-1xCO_2; Figs. 7b,e) are shown in Fig. 7 in a manner analogous to the nitrate and N^* analysis in Figs. 5 and 6. In both cases, spring chlorophyll is enhanced and summer chlorophyll is reduced under 2xCO_2 (Figs. 7a,b,d,e). The enhanced spring chlorophyll is associated with the reduction in sea ice extent (SIE) (blue solid line for 1xCO_2 and blue dashed line for 2xCO_2 in Fig. 7), which increases the shortwave flux into the ocean surface relative to that in the present-day climate. While both experiments with preindustrial N fluxes and contemporary ANFs exhibit these increases in chlorophyll (Figs. 7a,b), the increased chlorophyll is more distinctive for the contemporary ANF case (Fig. 7c). The ANF-associated chlorophyll increase is particularly distinctive in the Eurasian shelf seas (65°–90°N, 20°–160°E), where the increase is nearly 50% larger than that without ANF ($+5.0 \times 10^{-2}$ mg m^{-3} for preindustrial N, $+7.5 \times 10^{-2}$ mg m^{-3} with contemporary N). This region was reported as a high-sensitivity region of increased net primary production simulated in an idealized experiment by considering doubled riverine N fluxes (Terhaar et al. 2019). These nitrate and chlorophyll responses support previous findings demonstrating that the Arctic Ocean is N-limited (Arrigo et al. 2012; Popova et al. 2012; Vancoppenolle et al. 2013) and agree with the simulation here (Lim et al. 2019a). Contrary to the spring results, the reduced chlorophyll response in summer (Figs. 7d,e) suggests that the enhanced spring bloom affects the surface nitrate availability in the following summer. While the ANF-associated impact on the spring chlorophyll is distinctive in the preindustrial case, the ANF-associated impact on the summer chlorophyll exhibits a positive anomaly in the Kara–Barents Seas and a negative anomaly in the Laptev, East Siberian, and Chukchi Seas (Fig. 7f).

Figure 8 summarizes the monthly chlorophyll concentration averaged in the pan-Arctic Ocean to further explore ANFs' effect on seasonal chlorophyll changes. The simulated monthly chlorophyll changes in both experiments show similar behaviors in response to the doubled CO_2 (i.e., chlorophyll increases in spring and decreases throughout summer and fall; Figs. 8a,b). As discussed above, this reflects the changes from the alleviated light limitation in spring to the exacerbated nutrient limitation in summer and fall. The ANF-associated effect derived by subtracting Fig. 8a from Fig. 8b also shows that the magnitude of the positive chlorophyll concentration responses is enhanced by ANFs, especially in May (Fig. 8c). The June chlorophyll decline associated with the doubled CO_2 is also attenuated with ANFs, suggesting that the increased N inventory
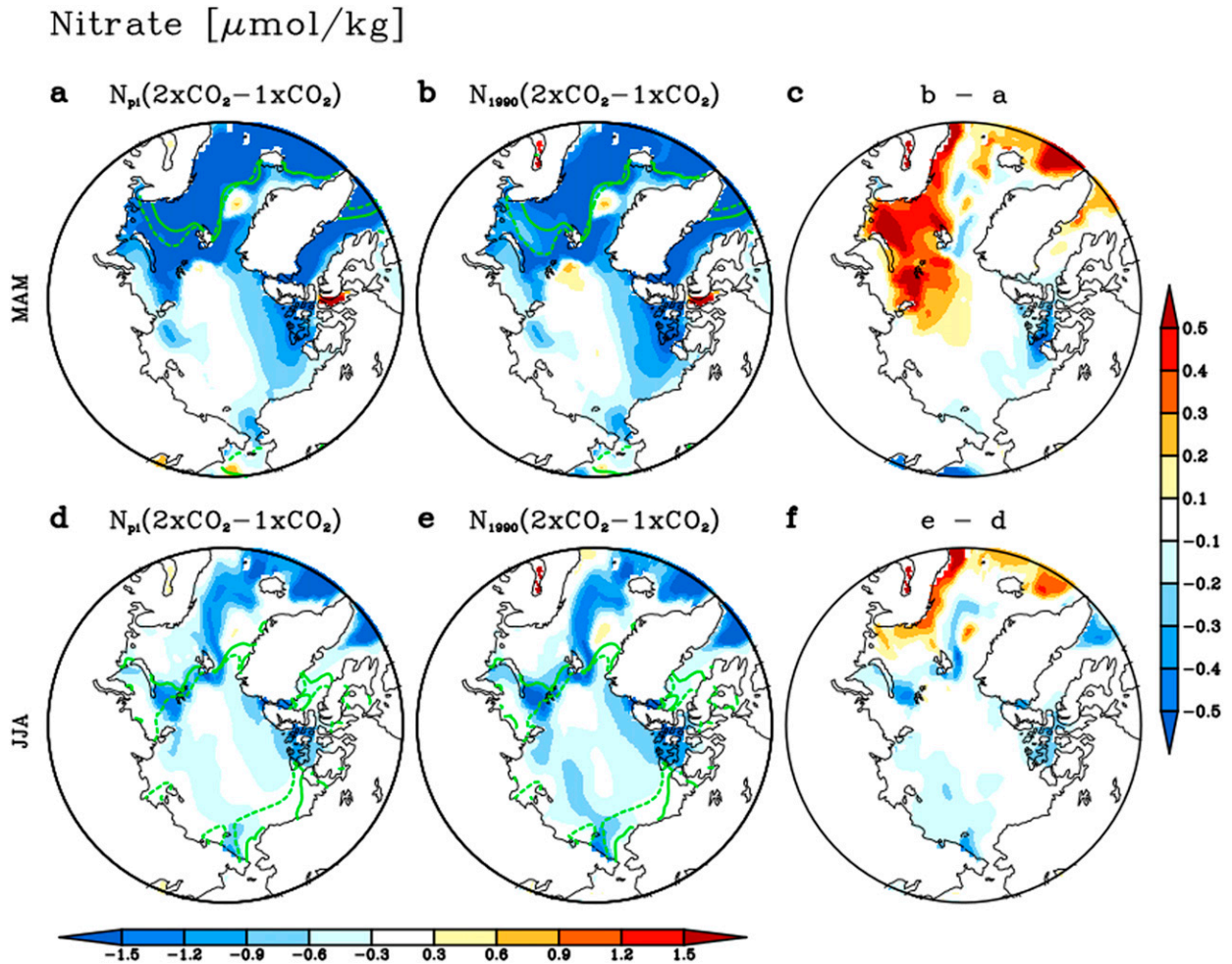
Nitrate [μmol/kg]

FIG. 5. Seasonal differences in simulated nitrate concentrations between present-day (1xCO$_2$) and future climate (2xCO$_2$) averaged up to 30 m ocean depth in (a),(b) spring (MAM) and (d),(e) summer (JJA) for nitrate sensitivity (a),(d) under preindustrial N flux and (b),(e) under contemporary N flux. (see lower color scale). (c),(f) Their differences (see right color scale). The contour lines denote the sea ice edge below 15% of the concentration of the present-day (solid) and future climates (dashed).

by ANFs delays the oligotrophic onset. Overall, the net impact of ANFs tempers the overall chlorophyll decreases associated with the doubled CO$_2$ by ~5%, from -2.82×10^{-2} mg m^{-3} in the preindustrial runs (N$_{Pi}$-2xCO$_2$–N$_{pi}$-1xCO$_2$) to -2.67×10^{-2} mg m^{-3} in the ANF runs (N$_{1990}$-2xCO$_2$ − N$_{1990}$-1xCO$_2$).

4. Additional shortwave heating enhanced by chlorophyll in future climate

The previous section shows nitrate and chlorophyll concentration changes under greenhouse warming; the impact of

ANF is that there is more chlorophyll in increased N forcing than in preindustrial N forcing. We examine the shortwave absorption rate (α_{sw}), which can give evidence of the role of increased chlorophyll in changing the light attenuation regardless of changes in shortwave flux input related to climate changes. The Manizza shortwave heating scheme is formulated as the multiplication of the shortwave flux reaching the ocean and its absorption rate (i.e., α_{sw}) (Manizza et al. 2005). Therefore, α_{sw} can be simply calculated by dividing the shortwave heating by the shortwave flux to isolate shortwave attenuation changes regardless of changes in the shortwave flux

TABLE 4. Climatological peaks (maximum in April and minimum in August) of simulated nitrate concentration (μmol kg^{-1}) up to 30 m depth of the ocean averaged in the pan-Arctic Ocean (averaged above 65°N) in the present day, the 10-member ensemble-mean future climate experiments, and their difference (impact of ANFs).

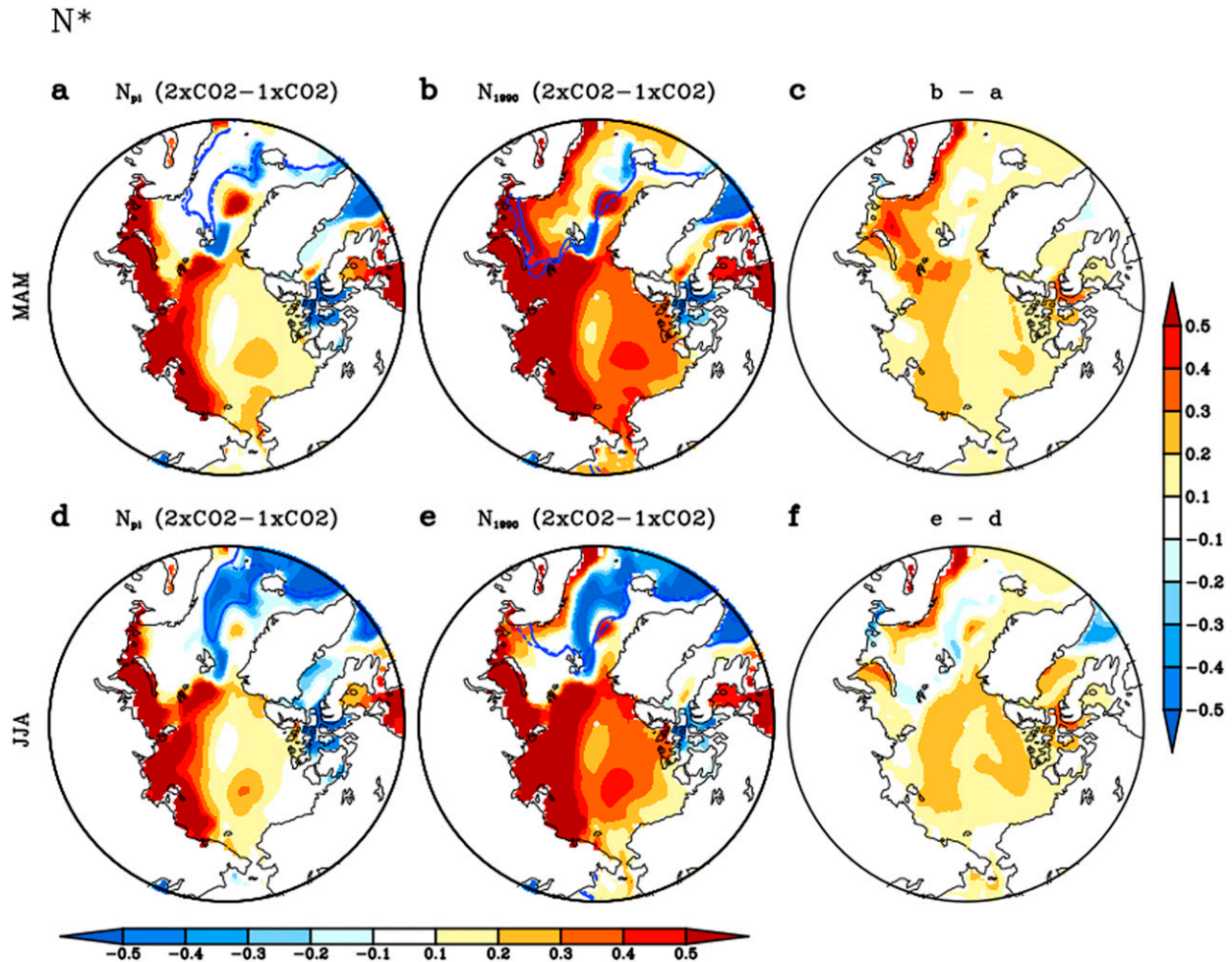|	N$_{pi}$-1xCO$_2$	N$_{pi}$-2xCO$_2$	N$_{1990}$-1xCO$_2$	N$_{1990}$-2xCO$_2$	Impact of ANFs
Maximum in April	5.39	4.53	6.17	5.39	0.08 (+9.8%)
Minimum in August	0.34	0.21	0.6	0.45	−0.01 (−11%)

N*

FIG. 6. Seasonal differences in simulated N^*, where $N^* = [NO_3] - 16 \times [PO_4^{3-}]$, between the present-day ($1 \times CO_2$) and future climate ($2 \times CO_2$) averaged up to 30 m ocean depth in (a),(b) spring (MAM) and (d),(e) summer (JJA) for N^* sensitivity (a),(d) under preindustrial N flux and (b),(e) under contemporary N flux (see lower color scale). (c),(f) Their differences (right color scale). The contour lines denote the zero N^* in the $1 \times CO_2$ (solid) and $2 \times CO_2$ (dashed) experiments.

input (Lim et al. 2019a). Since α_{sw} varies as a function of chlorophyll (Manizza et al. 2005; Lim et al. 2019a), the increase in chlorophyll (Figs. 7c,f) can lead to an increase in α_{sw}.

Figure 9 shows α_{sw} under greenhouse warming, integrated over the first 30 m to represent the surface layer. In spring, the model simulates increased mean chlorophyll concentrations in the Kara–Barents and East Siberian–Chukchi Seas (Figs. 7a,b), which enhances α_{sw} in both experiments (Figs. 9a,b). With preindustrial N external forcing, α_{sw} is increased by about 0.88% in the Kara–Barents Seas (70°–80°N, 30°–70°E) and by around 0.84% in the East Siberian–Chukchi Seas (65°–80°N, 160°E–160°W). With contemporary N external forcing, α_{sw} is further increased by approximately 1.00% in the Kara–Barents Seas and by about 1.18% in the East Siberian–Chukchi Seas due to an enhanced chlorophyll response. Figure 9c shows the impact of ANFs; α_{sw} is increased by about 0.30% in the Kara–Barents Seas and by around 0.16% in the East Siberian–Chukchi Seas. In summer, the model simulates decreases in

mean chlorophyll concentration over the pan-Arctic region in the future climate (Figs. 7d,e), which reduces α_{sw} in both experiments (Figs. 9d,e). In the pan-Arctic region, α_{sw} is decreased by approximately -0.79% in summer in the preindustrial N flux simulation and by about -0.73% in the contemporary N flux simulation. The impact of ANFs on α_{sw} (approximately $+0.24\%$), as shown in Fig. 9f, is notably enhanced in the Kara–Barents Seas, where mean chlorophyll is driven by human-induced N flux increases in the future climate (Fig. 7f). The increased chlorophyll bloom can explain the α_{sw} increase manifested near the Kara–Barents Seas in the current experiments.

The shortwave heating responses (as a result of the feedback processes between α_{sw} and increased shortwave flux input related to the sea ice melting) are shown in Fig. 10. Regardless of N flux forcing, shortwave heating is enhanced under greenhouse warming in both spring and summer (Figs. 10a,b,d,e) because greenhouse warming melts sea ice and thus reduces
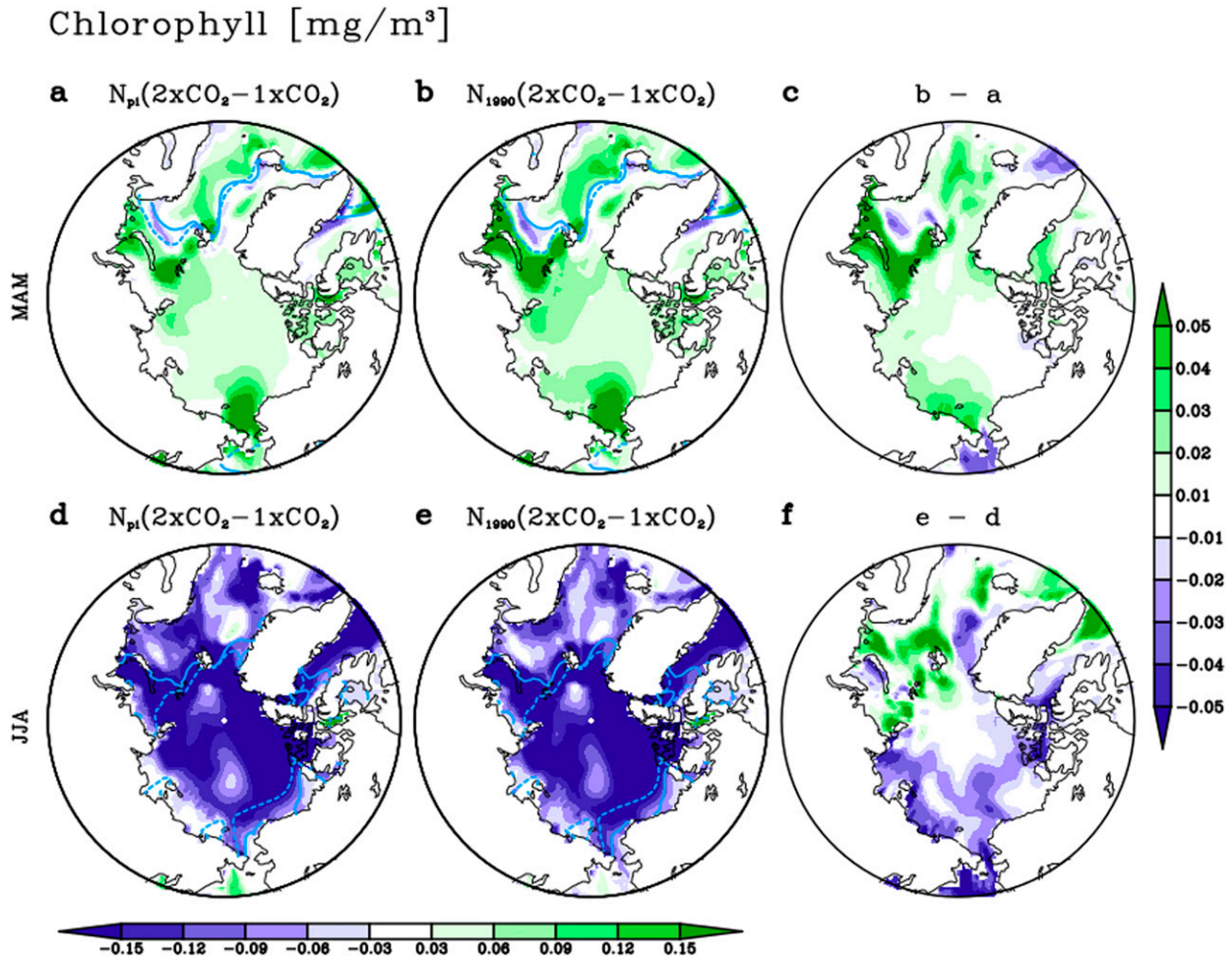
Chlorophyll [mg/m³]

FIG. 7. Seasonal differences in simulated chlorophyll concentration between the present-day ($1xCO_2$) and future climate ($2xCO_2$) averaged up to 30 m ocean depth in (a),(b) spring (MAM) and (d),(e) summer (JJA) for chlorophyll sensitivity (a),(d) under preindustrial N flux and (b),(e) under contemporary N flux (see lower color scale) (c),(f) Their differences (see right color scale). The contour lines denote the sea ice edge below 15% of the concentration of the present-day (solid) and future climates (dashed).

surface albedo, thereby allowing more shortwave flux input into the Arctic Ocean. In addition, ANFs enhance shortwave heating (Figs. 10c,f). The intensified α_{sw} due to the increased N forcing drives more attenuation at the given amount of the shortwave flux. In this simulation, ANFs enhance the annual shortwave heating by about $0.2\,\mathrm{W\,m}^{-2}$ (18%) from $0.9\,\mathrm{W\,m}^{-2}$ in N_{pi}-$2xCO_2$ minus N_{pi}-$1xCO_2$ to $1.1\,\mathrm{W\,m}^{-2}$ in N_{1990}-$2xCO_2$ minus N_{1990}-$1xCO_2$ in the pan-Arctic Ocean. The reduction in the sub-ice chlorophyll in JJA (Fig. 7f) seems to be a minor factor in this positive shortwave heating response in JJA. Thus, the negative nitrate response in the pan-Arctic Ocean shown in Figs. 5d and 5e is caused by the enhanced consumption of phytoplankton in MAM and decreased vertical mixing enhanced by shortwave heating in the upper ocean, which can be a major factor leading to the negative sub-ice chlorophyll response (Fig. 7f).

The vertical structure of the shortwave heating and related temperature in the pan-Arctic Ocean is shown in Fig. 11. The monthly shortwave heating response is represented in the

upper 30 m by increasing CO_2 (Figs. 11a,b). The positive chlorophyll anomaly (Figs. 7c,f) and related α_{sw} increase (Figs. 9c,f) induced by the ANFs enhance the net shortwave heating (Fig. 11c). Accordingly, the temperature response in the upper ocean due to the doubled CO_2 in the pan-Arctic Ocean is further enhanced by the shortwave heating (Figs. 11d–f). The mean ocean temperature in the upper 30 m, averaged from July to September (JAS), increases by 1.0 K (81.4%) with the N fluxes and 1.1 K (92.7%) with the contemporary N fluxes. The impact of ANF shows 0.1 K (11%) to be the strongest net temperature warming in the upper 30 m in JAS (Fig. 11f).

5. Impact of ANF amplifying Arctic warming

In fully coupled climate models considering the marine chlorophyll interaction, the upper-ocean temperature can be modified by changing the biologically induced absorption of solar radiation (Marzeion et al. 2005; Anderson et al. 2009;
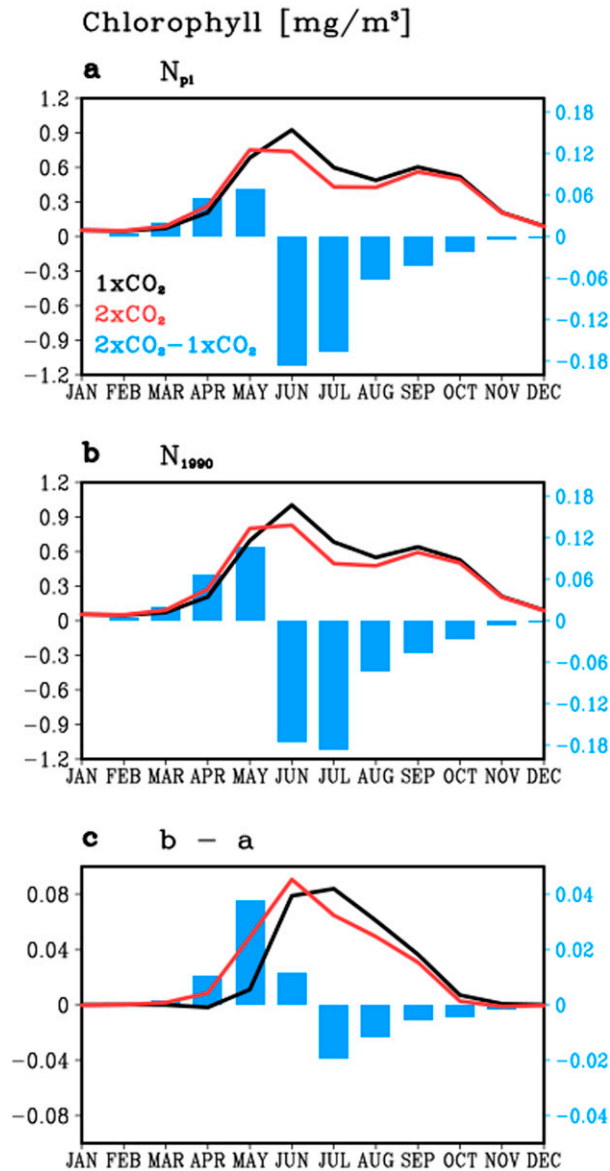
Chlorophyll [mg/m³]

FIG. 8. Seasonal cycle of chlorophyll concentration: (a) N_{pi}-1xCO_2 (black line), N_{pi}-2xCO_2 (red line), and their difference (blue bars); (b) N_{1990}-1xCO_2 (black line), N_{1990}-2xCO_2 (red line), and their difference (blue bars); and (c) N_{1990}-1xCO_2 − N_{pi}-1xCO_2 (black line), N_{1990}-2xCO_2 − N_{pi}-2xCO_2 (red line), and their difference (blue bars).

Lengaigne et al. 2009; Park et al. 2015; Lim et al. 2019b; Séférian et al. 2019). In particular, Lengaigne et al. (2009) assessed Arctic chlorophyll-associated biogeophysical feedback processes, which trap additional shortwave fluxes in the upper layer of the ocean and induce Arctic warming. Park et al. (2015) and Lim et al. (2019b) further suggested that Arctic warming is amplified by enhanced shortwave trapping under greenhouse warming. In this sense, as shown in section 4, the increasing light attenuation (i.e., α_{sw}) and enhanced shortwave heating can exacerbate Arctic warming.

The impact of the ANFs on the seasonal surface air temperature (SAT), surface air pressure (SAP), sea ice concentration (SIC), and sea ice thickness (SIT) responses under greenhouse warming is shown in Fig. 12. ANFs induce significantly positive surface temperature anomalies in the Arctic Ocean, particularly within the Eurasian shelf seas, which warm by about 0.9°C in winter (+16%) (contours in Fig. 12a). These warming patterns are evident across all seasons. Consisting of biophysical feedback in previous studies, ANF-associated biophysical feedback reduces the Arctic SIC (shading in Fig. 12a) and SIT (shading in Fig. 12b), most strongly near the Eurasian shelf seas. The decreases in the annual mean SIC and SIT are approximately −2.23% (−17%) and −3.2 cm (−16%) in the Eurasian shelf seas, where the values outside the parentheses are the absolute changes and the values in the parentheses are the percentage changes relative to the mean values during the contemporary period. The region of maximum impact for temperature and sea ice corresponds closely to positive ANF-associated chlorophyll anomalies (Figs. 7c,f), α_{sw} (Figs. 9c,f), and shortwave heating (Figs. 10c,f) in a manner consistent with shortwave feedback.

ANF-associated temperature and sea ice changes exhibit a seasonality wherein ANF impacts are strongest in December–February (DJF) compared with those in the other seasons. Contrary to the pan-Arctic surface warming associated with biophysical feedback in previous studies, the amplitude of Arctic warming by ANFs in this study is strongest near the Kara–Barents Seas (70°–80°N, 30°–70°E) at about +1.2 K (14%) in DJF. In this region, the reduction in the SIC is also strongest at −5.9% (−24.5%) in DJF. The sea ice melting is distinctive in winter near the marginal sea ice zone, which is closely related to the location of surface temperature warming. The sea ice melting in winter allows the active release of oceanic heat into the overlying cold atmosphere, which enhances surface warming in the atmosphere. By contrast, in summer, the ocean sinks the heat flux from the relatively warm atmosphere in the upper ocean, and this heat is utilized to melt the sea ice. This seasonality of the Arctic air–sea interaction drives the seasonal variation of the Arctic warming response; this finding is consistent with those of previous studies on the role of sea ice loss in Arctic amplification (Deser et al. 2010; Screen and Simmonds 2010; Tietsche et al. 2011) and biogeophysical feedback processes (Park et al. 2015; Lim et al. 2019b). The simulated impacts of ANFs on the future climate with uncertainty from internal variabilities at given N forcing, summarized in Table 5, are relatively small in midlatitudes but significant in the Arctic region, possibly due to strong local positive feedback.

Unlike that in the Eurasian shelf seas, the sea ice near the East Beaufort Sea increases modestly in response to the ANF-associated effects. Freezing in this area is associated with a positive Arctic Oscillation (AO)-like pattern of SAP in DJF and MAM (contour in Fig. 12b). The low pressure center of the positive AO-like pattern is located in the strongest sensitivity of sea ice responses in the Eurasian shelf seas. This sensitivity arises from additional oceanic heat release resulting from the additional open-ocean area, which in turn drives a low pressure system and in turn westerly wind
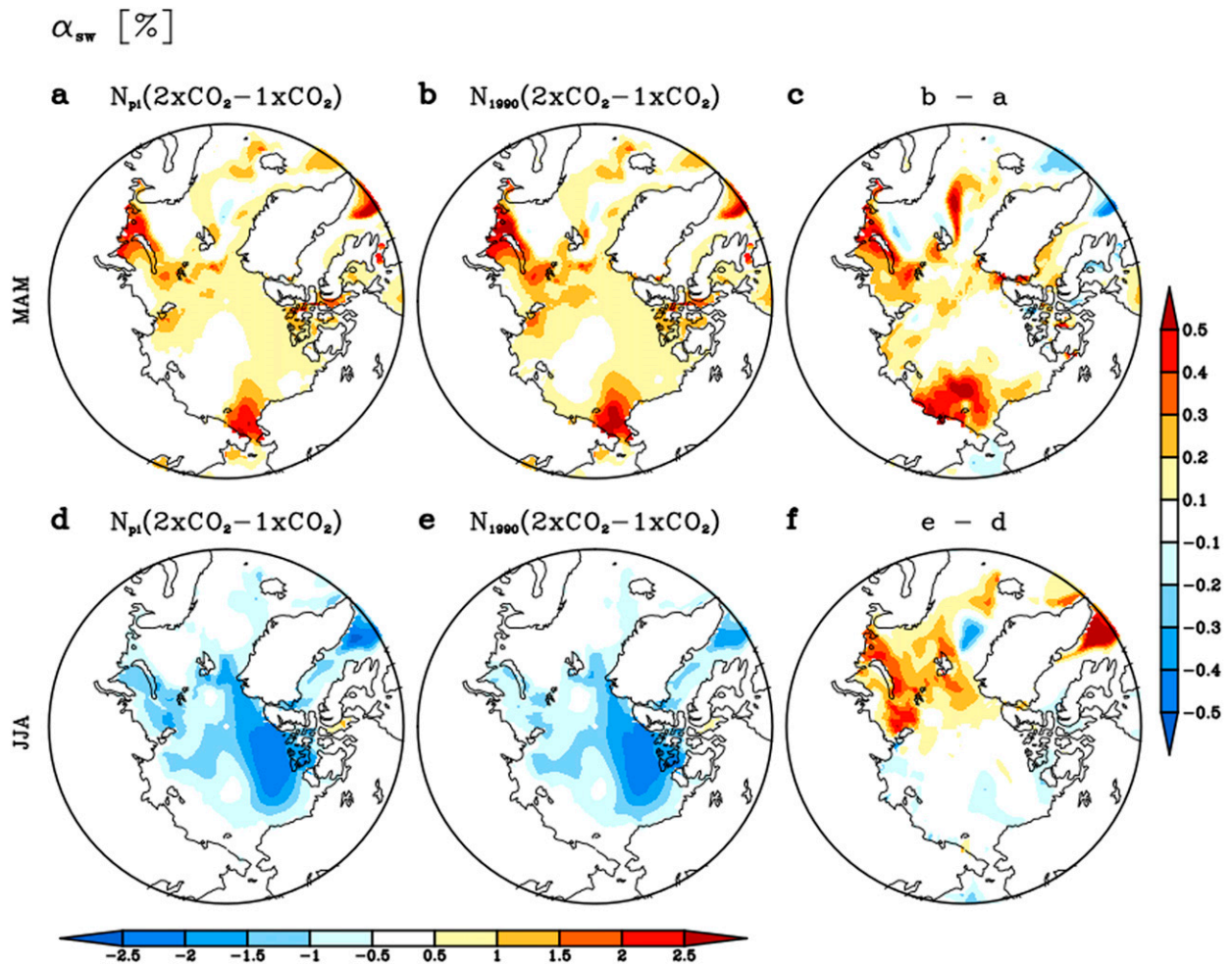
α_{sw} [%]

FIG. 9. Seasonal differences in simulated shortwave absorption rate (α_{sw}) between the present-day ($1xCO_2$) and future climate ($2xCO_2$) averaged up to 30 m ocean depth in (a),(b) spring (MAM) and (d),(e) summer (JJA) for α_{sw} sensitivity (a),(d) under preindustrial N flux and (b),(e) under contemporary N flux (see lower color scale). (c),(f) Their differences (see right color scale).

across the Chukchi Sea moving sea ice toward the East Beaufort Sea.

6. Summary and discussion

This study shows how an increased background of allochthonous N considering river and atmospheric depositions as the contemporary state affects biogeochemical processes and the Arctic climate. Arctic chlorophyll, which is strongly controlled by N, can be enhanced by increased N fluxes. The larger nutrient inventory and higher N fluxes can play a role in enhancing spring blooms under greenhouse warming. This chlorophyll fertilization enhances the light attenuation at given shortwave flux inputs (i.e., α_{sw}) in the Eurasian shelf seas. The additional net shortwave heating in the surface layer of the Arctic Ocean enhances sea ice melting, inducing positive ice–albedo feedback, and additional surface warming. The schematic in Fig. 13 shows how anthropogenic N forcing intensifies Arctic warming.

Extended from previous studies (Lengaigne et al. 2009; Park et al. 2015; Lim et al. 2019a,b), the present study assesses how ANFs via rivers and atmospheric deposition affect the Arctic climate through shortwave feedback. While previous studies considered only single human influences of CO_2, this study takes into account human-induced increases in CO_2 and N fluxes in the future climate sensitivity of the Arctic. The primary result shows that accurate N inventories should be used when assessing climate change in the Arctic (Table 2). The Arctic ecosystem is strongly controlled by the N inventory, which can be intensified in the future climate via enhanced autochthonous summer oligotrophy (Duce et al. 2008; Tremblay and Gagnon 2009; Wassmann and Reigstad 2011; Popova et al. 2012; Vancoppenolle et al. 2013; Lim et al. 2019a,b). If chlorophyll is fertilized under ANFs, Arctic warming will be further amplified (Fig. 13); that impact could be stronger in reality than the present study because the simulated chlorophyll concentration in the Arctic Ocean is still underestimated in the present experiment (N_{1990}-$1xCO_2$) despite considering
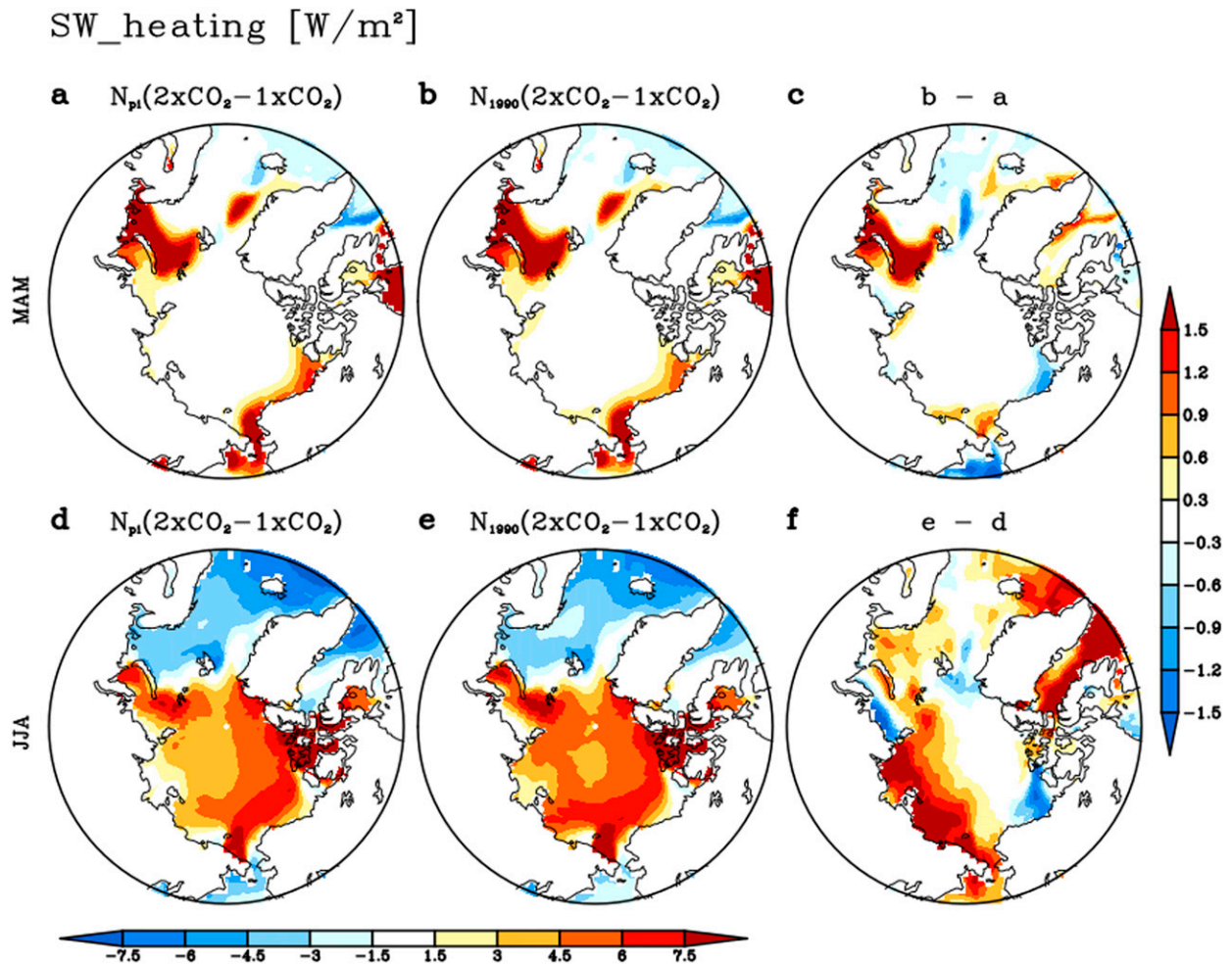
SW_heating [W/m²]

FIG. 10. Seasonal differences in simulated shortwave heating between the present-day ($1xCO_2$) and future climate ($2xCO_2$) averaged up to 30 m ocean depth in (a),(b) spring (MAM) and (d),(e) summer (JJA) for shortwave heating sensitivity (a),(d) under preindustrial N flux and (b),(e) under contemporary N flux (see lower color scale). (c),(f) Their differences (see right color scale).

the ANFs (Table 2). Therefore, as previously suggested, Arctic warming, amplified by biogeophysical feedback within closed marine N cycles (Park et al. 2015), can be further amplified by ANFs. In this sense, the human-induced N forcing and associated chlorophyll–shortwave feedback could be significantly altered in the Arctic Ocean.

Future projections of CMIP5 Earth system models (ESM) use fixed climatological values of N fluxes, and only a few ESMs include biogeophysical feedback. CMIP6 strongly recommends the use of either N deposition changes based on interactive atmospheric chemistry or prescription of chemical transport model results, which will give new insights for understanding future Arctic ecosystem response and climate sensitivity (Jones et al. 2016). However, despite the consideration for both biogeophysical feedback and ANFs in the present study, the forcing of Arctic N fluxes has uncertainty: the uncertainty of estimates for the present-day climate in the larger Arctic river N fluxes of 2.64 TgN yr^{-1} and in smaller global N fluxes of 35 Tg yr^{-1} estimated by Green et al. (2004)

compared to the six greatest Arctic river N fluxes 1.26 TgN yr^{-1} Holmes et al. (2012) and the global N fluxes 54 Tg yr^{-1} estimated by van Drecht et al. (2001); the disregard of changes in reactivity from dissolved organic, organic, and particulate N; the seasonality of Arctic Ocean riverine N fluxes; the disregard of coastal permafrost melting and coastal erosion to consider high N delivery on the Siberian shelf (i.e., Kara, Laptev, and East Siberian Seas) where nitrate concentration in N_{1990}-$1xCO_2$ is underestimated (Holmes et al. 2008; Lantuit et al. 2012; Tank et al. 2012; Sánchez-García et al. 2014; Wegner et al. 2015; Fritz et al. 2017; Thibodeau et al. 2017; Brüchert et al. 2018); largely uncertain amounts of N fluxes in the future climate, which are particularly due to the uncertainty of nutrient measurements (Holmes et al. 2000; Holmes et al. 2001; Vancoppenolle et al. 2013) and model biases in simulating the river delivery of N, residence time of tracers, and precipitation (Bring et al. 2015; Jun et al. 2018; Lee et al. 2019; Liu et al. 2019); the uncertainty driven by the generalization of global ballast protection interior remineralization scheme into the
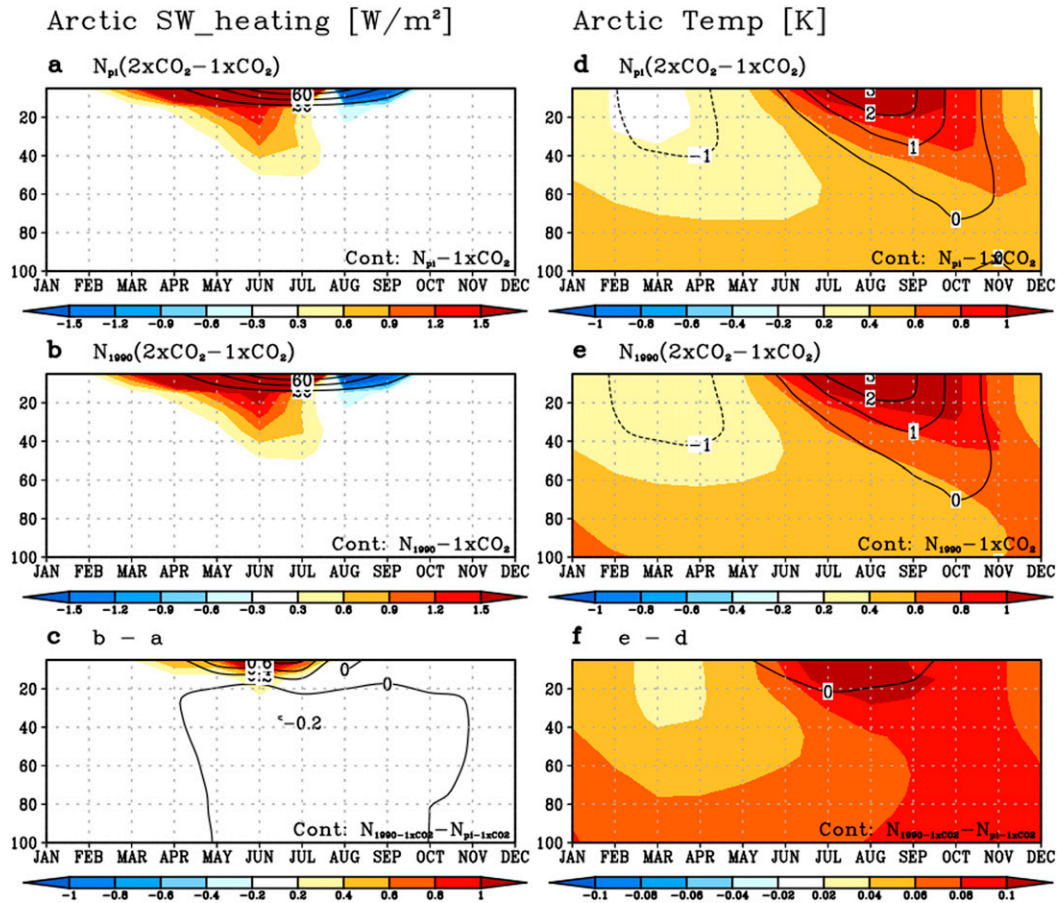
FIG. 11. Vertical structures of monthly climatology data of present-day (1xCO$_2$ runs; contours) and differences between the present-day and future climates (2xCO$_2$ − 1xCO$_2$ runs; shading) of the simulated (left) shortwave heating and (right) temperature in the Arctic Ocean (>65°N). Under greenhouse warming, (a) the shortwave heating response simulated by preindustrial amounts of N fluxes (N$_{pi}$-2xCO$_2$ − N$_{pi}$-1xCO$_2$), (b) as in (a), but simulated by anthropogenic amounts of N fluxes (N$_{1990}$-2xCO$_2$ − N$_{1990}$-1xCO$_2$), and (c) the impact of ANFs [i.e., (b) − (a)]. (d)–(f) As in (a)–(c), respectively, but for the simulated temperature.

regional Arctic Ocean specifically (Armstrong et al. 2002; Dunne et al. 2005, 2010); and finally quantifications of uncertainties depending on different N forcings from the rivers including seasonality (Holmes et al. 2012; McClelland et al. 2016) and adding the effect of N delivery from coastal erosion (Fritz et al. 2017).

The uncertainty of Arctic climate sensitivity may have been included due to the present experimental design, which is affected by a lack of dynamic dust (Evans et al. 2016), fixed sea salt aerosol amount (Paulot et al. 2020), disregard for light attenuation of colored dissolved organic matter (Stedmon et al. 2011; Kim et al. 2016), limited cloud feedback in this model due to negligible cloud changes around −0.05% in the Eurasian shelf seas, and relatively high and low sea ice concentration bias in spring and summer in GFDL-CM2.1-TOPAZ (Griffies et al. 2011) that can simulate the overestimated light limitation in spring and the overestimated nutrient limitation in summer. In addition, detection and attribution studies on the internal climate variability are further needed to achieve the robustness

of regional warming pattern in Eurasian shelf seas based on large ensemble experiments (Mori et al. 2014; Rodgers et al. 2015; Hyun et al. 2017; Kwon et al. 2018; Schlunegger et al. 2019), multimodel ensembles (Mori et al. 2019), and its time of emergence (Hyun et al. 2020; Schlunegger et al. 2020). Furthermore, other climate effects of anthropogenic N should be further considered: the creation of N$_2$O, which is a strong greenhouse gas (Stocker et al. 2013); NO$_x$ and NH$_3$ emission effects of cloud formation via cloud condensation nuclei and subsequent cooling (Shindell et al. 2009); and fertilization of N-limited terrestrial and marine ecosystems, which promotes cooling associated with the absorption of additional atmospheric CO$_2$ (Duce et al. 2008; Arneth et al. 2010).

Despite the above uncertainties, the present study represented the statistically significant Arctic warming effect of N flux. The significance over the Arctic internal variabilities is tested in the largest 10 ensembles, which were mostly investigated in three or five ensembles in Arctic chlorophyll feedback studies; The N forcing did not consider N flux changes with
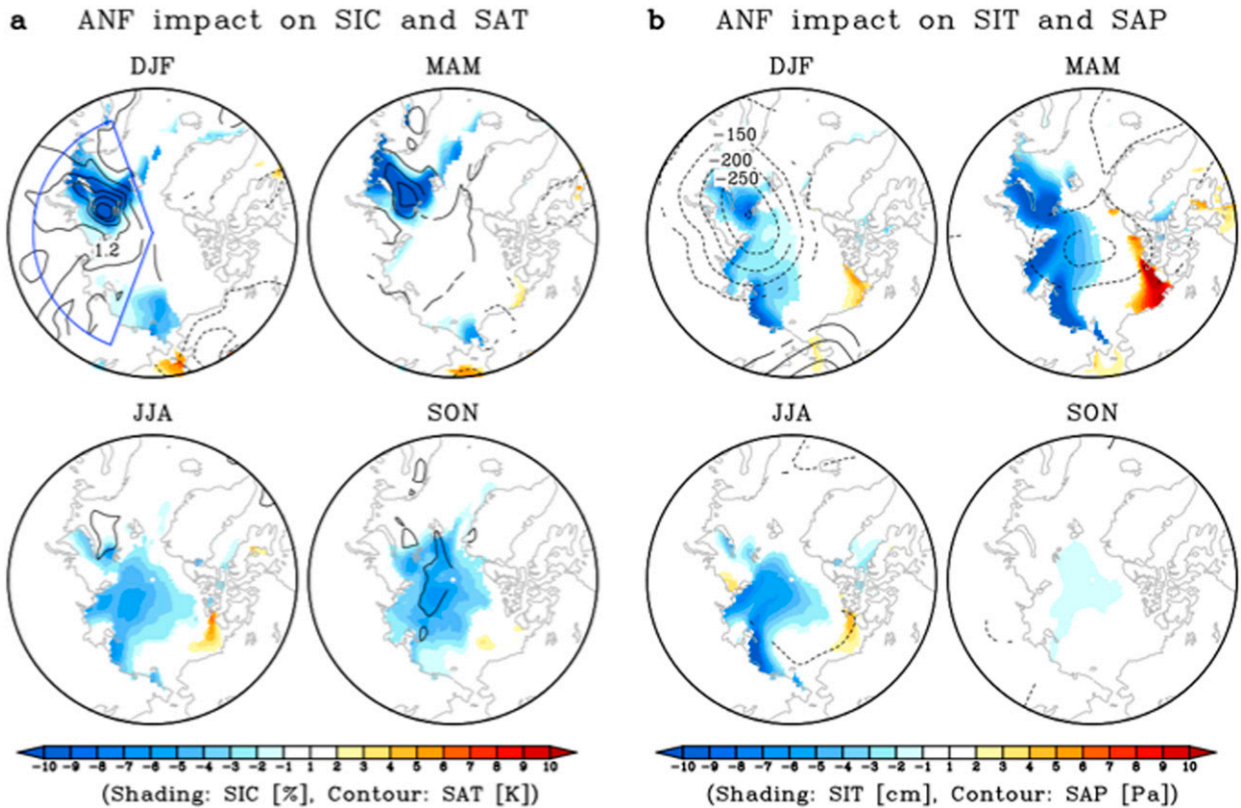
FIG. 12. Impact of ANFs on seasonal (a) SIC (shading) and SAT (contours with 0.4 K interval), and (b) SIT (shading) and surface air pressure (SAP; contours with 50 Pa interval). The impact of ANFs is estimated by a set of ANF runs [N_{1990}-2xCO_2 − N_{1990}-1xCO_2] minus a set of preindustrial N flux forcing runs [N_{pi}-2xCO_2 − N_{pi}-1xCO_2]. All shading and contours denote a statistically significant difference at a 95% confidence level. The blue section in (a) (labeled DJF) denotes the sensitive region against increased N fluxes in the Eurasian shelf seas (65°–90°N, 20°–160°E).

time, implying that the experimental design is a more conservative approach than the reality in which we expect many increases in N fluxes via increases in European agriculture, coastal erosion, thawing permafrost, and atmospheric emission

and deposition. The smaller amount of Arctic chlorophyll means simulated in GFDL-CM2.1-TOPAZ than observation could underestimate the enhanced shortwave absorption at the surface via N fluxes. The overestimated sea ice concentration simulated in

TABLE 5. Impact of ANFs under greenhouse warming on mean changes in annual mean and seasonal mean in SAT, SIC, SIE (>15% of SIC), and SIT averaged for areas of the Eurasian shelf seas (65°–90°N, 20°–160°E), pan-Arctic (65°–90°N), and midlatitudes (60°S–60°N). Parentheses denote percentage changes from a set of preindustrial N fluxes runs (N_{pi}-2xCO_2 − N_{pi}-1xCO_2) to a set of contemporary N fluxes runs (N_{1990}-2xCO_2 − N_{1990}-1xCO_2). Error range denotes ±1 standard deviation of 10 ensembles spread represented as internal variabilities.

|	Annual	DJF	MAM	JJA	SON
SAT in Eurasian shelf seas (K)	0.41 ± 0.23 (12% ± 6.6%)	0.94 ± 0.54 (16% ± 9.2%)	0.42 ± 0.21 (13% ± 6.2%)	0.07 ± 0.09 (8% ± 9.9%)	0.22 ± 0.18 (6% ± 5.0%)
SAT in midlatitudes (K)	−0.02 ± 0.03 (−1.0% ± 1.8%)	−0.02 ± 0.04 (−0.9% ± 2.7%)	−0.01 ± 0.03 (−0.7% ± 1.7%)	−0.02 ± 0.03 (−1.2% ± 1.9%)	−0.02 ± 0.02 (−1.4% ± 1.6%)
SIC in Eurasian shelf seas (%)	−2.23 ± 1.24 (−17% ± 9.5%)	−2.52 ± 1.5 (−23% ± 13.6%)	−2.66 ± 1.5 (−27% ± 15.1%)	−1.91 ± 1.05 (−13% ± 7.4%)	−1.84 ± 1.1 (−11% ± 6.7%)
SIT in Eurasian shelf seas (cm)	−3.3 ± 1.3 (−16% ± 6.5%)	−3.1 ± 1.7 (−13% ± 7.2%)	−6.6 ± 2.3 (−22% ± 7.9%)	−2.8 ± 0.9 (−14% ± 4.8%)	−0.5 ± 0.3 (−8.2% ± 5.0%)
SIT in pan-Arctic (cm)	−1.3 ± 1.1 (−6.9% ± 5.7%)	−1.4 ± 1.4 (−6.1% ± 6.3%)	−2.3 ± 1.9 (−8.2% ± 6.9%)	−1.3 ± 0.8 (−6.7% ± 4.1%)	−0.3 ± 0.3 (−4.3% ± 3.9%)
SIE in pan-Arctic (millions of km^2)	−0.18 ± 0.11 (−10.6% ± 6.9%)	−0.19 ± 0.12 (−15.1% ± 10.1%)	−0.17 ± 0.11 (−22.5% ± 14.7%)	−0.16 ± 0.12 (−7.1% ± 5.5%)	−0.17 ± 0.12 (−6.9% ± 5.0%)
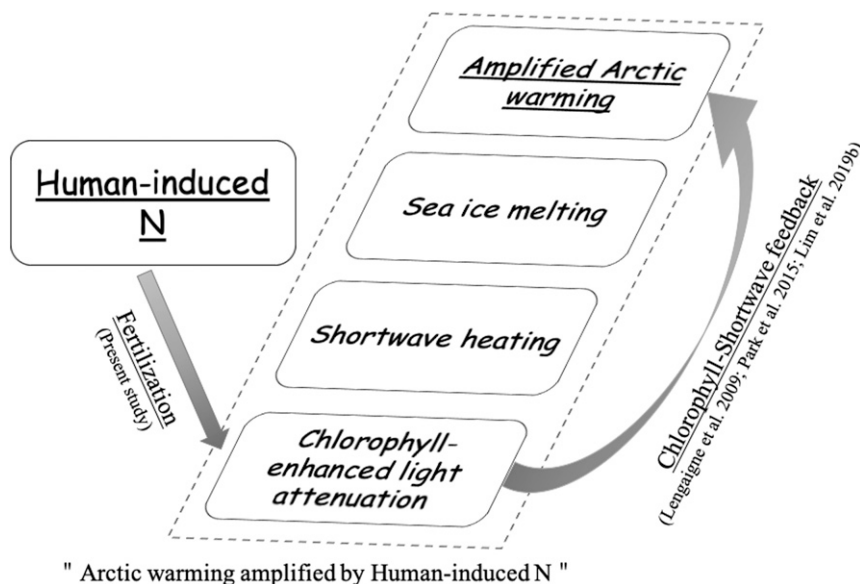
FIG. 13. Schematic figure of linkages in impact of human-induced N fluxes on Arctic warming amplification.

spring could limit the effect of N flux on the increased chlorophyll response in spring, which represented stronger than summer chlorophyll response. Such effects could therefore generate the underestimation of the effect of N fluxes on Arctic warming, which might be stronger than we estimated in the present study.

Nitrogen fluxes could become more important in the future for the Arctic Ocean than they currently are because of the intensifying stratification and its impact on N depletion and thus the ecosystem. The present results constitute a first step in quantifying the impact of ANFs on amplifying Arctic warming and its underlying mechanisms. Anthropogenic N fluxes increase chlorophyll and related shortwave feedback; this indicates the significances of considering the quantification in N fluxes and of simulating prognostics of N fluxes into the Arctic Ocean in climate projections. This may also be applicable to previous findings that future Arctic primary production will change in CMIP5 ESMs, but its diversity of sensitivity will depend on the diversity of the nitrate inventory (Popova et al. 2012; Vancoppenolle et al. 2013). Primary production increases by 11% when idealized riverine N in the pan-Arctic is doubled (Terhaar et al. 2019). Subsequently, considering increased N at temporal and spatial scales in future projections, a 30%–50% increase from West Siberia (Frey et al. 2007) can alter future phytoplankton biomass, primary production, and feedback processes in Arctic warming. This rich interplay between physical and biogeochemical processes is a promising area of future research.

REFERENCES

Anav, A., and Coauthors, 2013: Evaluating the land and ocean components of the global carbon cycle in the CMIP5 Earth system models. *J. Climate*, **26**, 6801–6843, https://doi.org/10.1175/JCLI-D-12-00417.1.

Anderson, D. M., P. M. Glibert, and J. M. Burkholder, 2002: Harmful algal blooms and eutrophication: Nutrient sources, composition, and consequences. *Estuaries*, **25**, 704–726, https://doi.org/10.1007/BF02804901.

Anderson, J. L., V. Balaji, A. J. Broccoli, and W. F. Cooke, 2004: The new GFDL global atmosphere and land model AM2-LM2: Evaluation with prescribed SST simulations. *J. Climate*, **17**, 4641–4673, https://doi.org/10.1175/JCLI-3223.1.

Anderson, W., A. Gnanadesikan, and A. Wittenberg, 2009: Regional impacts of ocean color on tropical Pacific variability. *Ocean Sci.*, **5**, 313–327, https://doi.org/10.5194/os-5-313-2009.

Antonov, J., R. Locarnini, T. Boyer, A. Mishonov, and H. Garcia, 2006: *Salinity.* Vol. 2, *World Ocean Atlas 2005*, NOAA Atlas NESDIS 62, 182 pp.

Armstrong, R. A., C. Lee, J. I. Hedges, S. Honjo, and S. G. Wakeham, 2002: A new, mechanistic model for organic carbon

fluxes in the ocean based on the quantitative association of POC with ballast minerals. *Deep-Sea Res. II*, **49**, 219–236, https://doi.org/10.1016/S0967-0645(01)00101-1.

Arneth, A., and Coauthors, 2010: Terrestrial biogeochemical feedbacks in the climate system. *Nat. Geosci.*, **3**, 525–532, https://doi.org/10.1038/ngeo905.

Arrigo, K. R., and G. L. van Dijken, 2011: Secular trends in Arctic Ocean net primary production. *J. Geophys. Res.*, **116**, C09011, https://doi.org/10.1029/2011JC007151.

——, and ——, 2015: Continued increases in Arctic Ocean primary production. *Prog. Oceanogr.*, **136**, 60–70, https://doi.org/10.1016/j.pocean.2015.05.002.

——, and Coauthors, 2012: Massive phytoplankton blooms under Arctic sea ice. *Science*, **336**, 1408, https://doi.org/10.1126/science.1215065.

Boyer, E. W., R. W. Howarth, J. N. Galloway, F. J. Dentener, P. A. Green, and C. J. Vörösmarty, 2006: Riverine nitrogen export from the continents to the coasts. *Global Biogeochem. Cycles*, **20**, GB1S91, https://doi.org/10.1029/2005GB002537.

Bring, A., and Coauthors, 2015: Implications of freshwater flux data from the CMIP5 multimodel output across a set of Northern Hemisphere drainage basins. *Earth's Future*, **3**, 206–217, https://doi.org/10.1002/2014EF000296.

Brüchert, V., and Coauthors, 2018: Carbon mineralization in Laptev and East Siberian Sea shelf and slope sediment. *Biogeosciences*, **15**, 471–490, https://doi.org/10.5194/bg-15-471-2018.

Cabré, A., I. Marinov, and S. Leung, 2015: Consistent global responses of marine ecosystems to future climate change across the IPCC AR5 Earth system models. *Climate Dyn.*, **45**, 1253–1280, https://doi.org/10.1007/s00382-014-2374-3.

Delworth, T. L., and Coauthors, 2006: GFDL's CM2 global coupled climate models. Part I: Formulation and simulation characteristics. *J. Climate*, **19**, 643–674, https://doi.org/10.1175/JCLI3629.1.

Deser, C., R. Tomas, M. Alexander, and D. Lawrence, 2010: The seasonal atmospheric response to projected Arctic sea ice loss in the late twenty-first century. *J. Climate*, **23**, 333–351, https://doi.org/10.1175/2009JCLI3053.1.

Diaz, R. J., and R. Rosenberg, 2008: Spreading dead zones and consequences for marine ecosystems. *Science*, **321**, 926–929, https://doi.org/10.1126/science.1156401.

Duce, R. A., and Coauthors, 2008: Impacts of atmospheric anthropogenic nitrogen on the open ocean. *Science*, **320**, 893–897, https://doi.org/10.1126/science.1150369.

Dunne, J. P., R. A. Armstrong, A. Gnanadesikan, and J. L. Sarmiento, 2005: Empirical and mechanistic models for the particle export ratio. *Global Biogeochem. Cycles*, **19**, GB4026, https://doi.org/10.1029/2004GB002390.

——, A. Gnanadesikan, J. L. Sarmiento, and R. D. Slater, 2010: Technical description of the prototype version (v0) of Tracers of Phytoplankton with Allometric Zooplankton (TOPAZ) ocean biogeochemical model as used in the Princeton IFMIP model. *Biogeosciences*, **7**, 1–22, https://doi.org/10.5194/bg-7-3593-2010.

——, B. Hales, and J. R. Toggweiler, 2012a: Global calcite cycling constrained by sediment preservation controls. *Global Biogeochem. Cycles*, **26**, GB3023, https://doi.org/10.1029/2010GB003935.

——, and Coauthors, 2012b: GFDL's ESM2 global coupled climate–carbon Earth system models. Part I: Physical formulation and baseline simulation characteristics. *J. Climate*, **25**, 6646–6665, https://doi.org/10.1175/JCLI-D-11-00560.1.

——, and Coauthors, 2013: GFDL's ESM2 global coupled climate–carbon Earth system models. Part II: Carbon system formu-

lation and baseline simulation characteristics. *J. Climate*, **26**, 2247–2267, https://doi.org/10.1175/JCLI-D-12-00150.1.

Evans, S., P. Ginoux, S. Malyshev, and E. Shevliakova, 2016: Climate–vegetation interaction and amplification of Australian dust variability. *Geophys. Res. Lett.*, **43**, 11 823–11 830, https://doi.org/10.1002/2016GL071016.

Fan, S.-M., W. J. Moxim, and H. Levy, 2006: Aeolian input of bioavailable iron to the ocean. *Geophys. Res. Lett.*, **33**, L07602, https://doi.org/10.1029/2005GL024852.

Frey, K. E., J. W. McClelland, R. M. Holmes, and L. C. Smith, 2007: Impacts of climate warming and permafrost thaw on the riverine transport of nitrogen and phosphorus to the Kara Sea. *J. Geophys. Res. Biogeosci.*, **112**, G04S58, https://doi.org/10.1029/2006JG000369.

Fritz, M., J. Vonk, and H. Lantuit, 2017: Collapsing Arctic coastlines. *Nat. Climate Change*, **7**, 6–7, https://doi.org/10.1038/nclimate3188.

Galloway, J. N., J. D. Aber, J. W. Erisman, S. P. Seitzinger, R. W. Howarth, E. B. Cowling, and B. J. Cosby, 2003: The nitrogen cascade. *BioScience*, **53**, 341–356, https://doi.org/10.1641/0006-3568(2003)053[0341:TNC]2.0.CO;2.

——, and Coauthors, 2004: Nitrogen cycles: Past, present, and future. *Biogeochemistry*, **70**, 153–226, https://doi.org/10.1007/s10533-004-0370-0.

——, and Coauthors, 2008: Transformation of the nitrogen cycle: Recent trends, questions, and potential solutions. *Science*, **320**, 889–892, https://doi.org/10.1126/science.1136674.

Garcia, H., R. Locarnini, T. Boyer, and J. Antonov, 2006a: *Dissolved Oxygen, Apparent Oxygen Utilization, and Oxygen Saturation*. Vol. 3, *World Ocean Atlas 2005*, NOAA Atlas NESDIS 63, 342 pp.

——, ——, ——, ——, and S. Levitus, 2006b: *Nutrients (Phosphate, Nitrate, Silicate)*. Vol. 4, *World Ocean Database 2005*, NOAA Atlas NESDIS 64, 396 pp.

——, and Coauthors, 2014: *Dissolved Inorganic Nutrients (Phosphate, Nitrate, Silicate)*. Vol. 4, *World Ocean Atlas 2013*, NOAA Atlas NESDIS 76, 25 pp.

Geider, R., H. MacIntyre, and T. Kana, 1997: Dynamic model of phytoplankton growth and acclimation: Responses of the balanced growth rate and the chlorophyll a:carbon ratio to light, nutrient-limitation and temperature. *Mar. Ecol. Prog. Ser.*, **148**, 187–200, https://doi.org/10.3354/meps148187.

Giese, B. S., and S. Ray, 2011: El Niño variability in Simple Ocean Data Assimilation (SODA), 1871–2008. *J. Geophys. Res.*, **116**, C02024, https://doi.org/10.1029/2010JC006695.

Green, P. A., C. J. Vörösmarty, M. Meybeck, J. N. Galloway, B. J. Peterson, and E. W. Boyer, 2004: Pre-industrial and contemporary fluxes of nitrogen through rivers: A global assessment based on typology. *Biogeochemistry*, **68**, 71–105, https://doi.org/10.1023/B:BIOG.0000025742.82155.92.

Griffies, S. M., 2012: Elements of the Modular Ocean Model (MOM). NOAA Geophysical Fluid Dynamics Laboratory/GFDL Ocean Group Tech. Rep. 7, 632 pp.

——, and Coauthors, 2011: The GFDL CM3 coupled climate model: Characteristics of the ocean and sea ice simulations. *J. Climate*, **24**, 3520–3544, https://doi.org/10.1175/2011JCLI3964.1.

Gruber, N., and J. L. Sarmiento, 1997: Global patterns of marine nitrogen fixation and denitrification. *Global Biogeochem. Cycles*, **11**, 235–266, https://doi.org/10.1029/97GB00077.

——, and J. N. Galloway, 2008: An Earth-system perspective of the global nitrogen cycle. *Nature*, **451**, 293–296, https://doi.org/10.1038/nature06592.

Hegglin, M., D. Kinnison, and J.-F. Lamarque, 2016: CCMI nitrogen surface fluxes in support of CMIP6–version 2.0. Earth System Grid Federation, accessed 2018, https://doi.org/10.22033/ESGF/input4MIPs.1125.

Holmes, R. M., B. J. Peterson, V. V. Gordeev, A. V. Zhulidov, M. Meybeck, R. B. Lammers, and C. J. Vörösmarty, 2000: Flux of nutrients from Russian rivers to the Arctic Ocean: Can we establish a baseline against which to judge future changes? Water Resour. Res., 36, 2309–2320, https://doi.org/10.1029/2000WR900099.

——, and Coauthors, 2001: Nutrient chemistry of the Ob' and Yenisey Rivers, Siberia: Results from June 2000 expedition and evaluation of long-term data sets. Mar. Chem., 75, 219–227, https://doi.org/10.1016/S0304-4203(01)00038-X.

——, J. W. McClelland, P. A. Raymond, B. B. Frazer, B. J. Peterson, and M. Stieglitz, 2008: Lability of DOC transported by Alaskan rivers to the Arctic Ocean. Geophys. Res. Lett., 35, L03402, https://doi.org/10.1029/2007GL032837.

——, and Coauthors, 2012: Seasonal and annual fluxes of nutrients and organic matter from large rivers to the Arctic Ocean and surrounding seas. Estuaries Coasts, 35, 369–382, https://doi.org/10.1007/s12237-011-9386-6.

Horowitz, L. W., and Coauthors, 2003: A global simulation of tropospheric ozone and related tracers: Description and evaluation of MOZART, version 2. J. Geophys. Res., 108, 4784, https://doi.org/10.1029/2002JD002853.

Hyun, S.-H., S.-W. Yeh, and J. Yoon, 2017: Reduction of internal climate variability in surface temperature due to sea-ice loss since the mid-21st century. Int. J. Climatol., 37, 5211–5216, https://doi.org/10.1002/joc.5146.

——, ——, S.-Y. Song, H.-S. Park, and B. P. Kirtman, 2020: Understanding intermodel diversity when simulating the time of emergence in CMIP5 climate models. Geophys. Res. Lett., 47, e2020GL087923, https://doi.org/10.1029/2020GL087923.

Jakobsson, M., 2002: Hypsometry and volume of the Arctic Ocean and its constituent seas. Geochem. Geophys. Geosyst., 3, 1–18, https://doi.org/10.1029/2001GC000302.

Jones, C. D., and Coauthors, 2016: The C4MIP experimental protocol for CMIP6. Geosci. Model Dev., 9, 2853–2880, https://doi.org/10.5194/gmd-9-2853-2016.

Jun, S.-Y., S.-J. Choi, and B.-M. Kim, 2018: Dynamical core in atmospheric model does matter in the simulation of Arctic climate. Geophys. Res. Lett., 45, 2805–2814, https://doi.org/10.1002/2018GL077478.

Key, R. M., and Coauthors, 2004: A global ocean carbon climatology: Results from global data analysis project (GLODAP). Global Biogeochem. Cycles, 18, GB4031, https://doi.org/10.1029/2004GB002247.

Kim, G. E., A. Gnanadesikan, and M.-A. Pradal, 2016: Increased surface ocean heating by colored detrital matter (CDM) linked to greater Northern Hemisphere ice formation in the GFDL CM2Mc ESM. J. Climate, 29, 9063–9076, https://doi.org/10.1175/JCLI-D-16-0053.1.

Kim, I.-N., K. Lee, N. Gruber, D. M. Karl, J. L. Bullister, S. Yang, and T.-W. Kim, 2014: Increasing anthropogenic nitrogen in the North Pacific Ocean. Science, 346, 1102–1106, https://doi.org/10.1126/science.1258396.

Krishnamurthy, A., J. K. Moore, C. S. Zender, and C. Luo, 2007: Effects of atmospheric inorganic nitrogen deposition on ocean biogeochemistry. J. Geophys. Res. Biogeosci., 112, G02019, https://doi.org/10.1029/2006JG000334.

Kwon, Y.-O., A. Camacho, C. Martinez, and H. Seo, 2018: North Atlantic winter eddy-driven jet and atmospheric blocking variability in the Community Earth System Model version 1 Large Ensemble simulations. Climate Dyn., 51, 3275–3289, https://doi.org/10.1007/s00382-018-4078-6.

Lamarque, J. F., and Coauthors, 2012: CAM-chem: Description and evaluation of interactive atmospheric chemistry in the Community Earth System Model. Geosci. Model Dev., 5, 369–411, https://doi.org/10.5194/gmd-5-369-2012.

Lantuit, H., W. H. Pollard, N. Couture, M. Fritz, L. Schirrmeister, H. Meyer, and H. W. Hubberten, 2012: Modern and late Holocene retrogressive thaw slump activity on the Yukon coastal plain and Herschel Island, Yukon territory, Canada. Permafr. Periglac. Process., 23, 39–51, https://doi.org/10.1002/ppp.1731.

Large, W. G., and S. G. Yeager, 2004: Diurnal to decadal global forcing for ocean and sea-ice models: The data sets and flux climatologies. NCAR Tech. Note NCAR/TN-460+STR, 112 pp., http://doi.org/10.5065/D6KK98Q6.

Laufkötter, C., and Coauthors, 2015: Drivers and uncertainties of future global marine primary production in marine ecosystem models. Biogeosciences, 12, 6955–6984, https://doi.org/10.5194/bg-12-6955-2015.

Lauvset, S. K., and Coauthors, 2016: New global interior ocean mapped climatology: the 1° × 1° GLODAP version 2. Earth Syst. Sci. Data, 8, 325–340, https://doi.org/10.5194/essd-8-325-2016.

Lee, M., E. Shevliakova, C. A. Stock, S. Malyshev, and P. C. D. Milly, 2019: Prominence of the tropics in the recent rise of global nitrogen pollution. Nat. Commun., 10, 1437, https://doi.org/10.1038/s41467-019-09468-4.

Lee, Y. J., and Coauthors, 2016: Net primary productivity estimates and environmental variables in the Arctic Ocean: An assessment of coupled physical-biogeochemical models. J. Geophys. Res. Oceans, 121, 8635–8669, https://doi.org/10.1002/2016JC011993.

Le Fouest, V., M. Babin, and J. É. Tremblay, 2013: The fate of riverine nutrients on Arctic shelves. Biogeosciences, 10, 3661–3677, https://doi.org/10.5194/bg-10-3661-2013.

——, M. Manizza, B. Tremblay, and M. Babin, 2015: Modelling the impact of riverine DON removal by marine bacterioplankton on primary production in the Arctic Ocean. Biogeosciences, 12, 3385–3402, https://doi.org/10.5194/bg-12-3385-2015.

Lengaigne, M., G. Madec, L. Bopp, C. Menkes, O. Aumont, and P. Cadule, 2009: Bio-physical feedbacks in the Arctic Ocean using an Earth system model. Geophys. Res. Lett., 36, L21602, https://doi.org/10.1029/2009GL040145.

Lim, H.-G., J.-Y. Park, and J.-S. Kug, 2018: Impact of chlorophyll bias on the tropical Pacific mean climate in an Earth system model. Climate Dyn., 51, 2681–2694, https://doi.org/10.1007/s00382-017-4036-8.

——, J.-S. Kug, and J.-Y. Park, 2019a: Biogeophysical feedback of phytoplankton on the Arctic climate. Part I: Impact of nonlinear rectification of interactive chlorophyll variability in the present-day climate. Climate Dyn., 52, 5383–5396, https://doi.org/10.1007/s00382-018-4450-6.

——, ——, and ——, 2019b: Biogeophysical feedback of phytoplankton on Arctic climate. Part II: Arctic warming amplified by interactive chlorophyll under greenhouse warming. Climate Dyn., 53, 3167–3180, https://doi.org/10.1007/s00382-019-04693-5.

Lin, S.-J., 2004: A "vertically Lagrangian" finite-volume dynamical core for global models. Mon. Wea. Rev., 132, 2293–2307, https://doi.org/10.1175/1520-0493(2004)132<2293:AVLFDC>2.0.CO;2.

Liu, X., J. P. Dunne, C. A. Stock, M. J. Harrison, A. Adcroft, and L. Resplandy, 2019: Simulating water residence time in the coastal ocean: A global perspective. Geophys. Res. Lett., 46, 13 910–13 919, https://doi.org/10.1029/2019GL085097.

Locarnini, R., and Coauthors, 2006: *Temperature*. Vol. 1, *World Ocean Atlas 2005*, NOAA Atlas NESDIS 61, 182 pp.

Manizza, M., C. Le Quéré, A. J. Watson, and E. T. Buitenhuis, 2005: Bio-optical feedbacks among phytoplankton, upper ocean physics and sea-ice in a global model. *Geophys. Res. Lett.*, **32**, L05603, https://doi.org/10.1029/2004GL020778.

Marzeion, B., A. Timmermann, R. Murtugudde, and F.-F. Jin, 2005: Biophysical feedbacks in the tropical Pacific. *J. Climate*, **18**, 58–70, https://doi.org/10.1175/JCLI3261.1.

McClelland, J. W., R. M. Holmes, B. J. Peterson, and M. Stieglitz, 2004: Increasing river discharge in the Eurasian Arctic: Consideration of dams, permafrost thaw, and fires as potential agents of change. *J. Geophys. Res.*, **109**, D18102, https://doi.org/10.1029/2004JD004583.

——, and Coauthors, 2016: Particulate organic carbon and nitrogen export from major Arctic rivers. *Global Biogeochem. Cycles*, **30**, 629–643, https://doi.org/10.1002/2015GB005351.

Middelburg, J. J., K. Soetaert, P. M. J. Herman, and C. H. R. Heip, 1996: Denitrification in marine sediments: A model study. *Global Biogeochem. Cycles*, **10**, 661–673, https://doi.org/10.1029/96GB02562.

Milly, P. C. D., and A. B. Shmakin, 2002: Global modeling of land water and energy balances. Part I: The Land Dynamics (LaD) model. *J. Hydrometeor.*, **3**, 283–299, https://doi.org/10.1175/1525-7541(2002)003<0283:GMOLWA>2.0.CO;2.

Min, S.-K., X. Zhang, and F. Zwiers, 2008: Human-induced Arctic moistening. *Science*, **320**, 518–520, https://doi.org/10.1126/science.1153468.

Morel, A., 1988: Optical modeling of the upper ocean in relation to its biogenous matter content (case I waters). *J. Geophys. Res.*, **93**, 10 749–10 768, https://doi.org/10.1029/JC093iC09p10749.

——, and D. Antoine, 1994: Heating rate within the upper ocean in relation to its bio-optical state. *J. Phys. Oceanogr.*, **24**, 1652–1665, https://doi.org/10.1175/1520-0485(1994)024<1652:HRWTUO>2.0.CO;2.

Mori, M., M. Watanabe, H. Shiogama, J. Inoue, and M. Kimoto, 2014: Robust Arctic sea-ice influence on the frequent Eurasian cold winters in past decades. *Nat. Geosci.*, **7**, 869–873, https://doi.org/10.1038/ngeo2277.

——, Y. Kosaka, M. Watanabe, H. Nakamura, and M. Kimoto, 2019: A reconciled estimate of the influence of Arctic sea-ice loss on recent Eurasian cooling. *Nat. Climate Change*, **9**, 123–129, https://doi.org/10.1038/s41558-018-0379-3.

Müller, D., and Coauthors, 2015: The Ocean Colour Climate Change Initiative: I. A methodology for assessing atmospheric correction processors based on in-situ measurements. *Remote Sens. Environ.*, **162**, 242–256, https://doi.org/10.1016/j.rse.2013.11.026.

Murray, R. J., 1996: Explicit generation of orthogonal grids for ocean models. *J. Comput. Phys.*, **126**, 251–273, https://doi.org/10.1006/jcph.1996.0136.

Pabi, S., G. L. van Dijken, and K. R. Arrigo, 2008: Primary production in the Arctic Ocean, 1998–2006. *J. Geophys. Res.*, **113**, C08005, https://doi.org/10.1029/2007JC004578.

Park, J. Y., J. S. Kug, J. Badera, R. Rolph, and M. Kwon, 2015: Amplified Arctic warming by phytoplankton under greenhouse warming. *Proc. Natl. Acad. Sci. USA*, **112**, 5921–5926, https://doi.org/10.1073/pnas.1416884112.

Paulot, F., D. Paynter, M. Winton, P. Ginoux, M. Zhao, and L. W. Horowitz, 2020: Revisiting the impact of sea salt on climate sensitivity. *Geophys. Res. Lett.*, **47**, e2019GL085601, https://doi.org/10.1029/2019GL085601.

Peterson, B. J., and Coauthors, 2002: Increasing river discharge to the Arctic Ocean. *Science*, **298**, 2171–2173, https://doi.org/10.1126/science.1077445.

Popova, E. E., and Coauthors, 2012: What controls primary production in the Arctic Ocean? Results from an intercomparison of five general circulation models with biogeochemistry. *J. Geophys. Res.*, **117**, C00D12, https://doi.org/10.1029/2011JC007112.

Rayner, N. A., D. E. Parker, E. B. Horton, C. K. Folland, L. V. Alexander, D. P. Rowell, E. C. Kent, and A. Kaplan, 2003: Global analyses of sea surface temperature, sea ice, and night marine air temperature since the late nineteenth century. *J. Geophys. Res.*, **108**, 4407, https://doi.org/10.1029/2002JD002670.

Redfield, A. C., 1963: The influence of organisms on the composition of seawater. *The Sea*, Vol. 2, M. N. Hill, Ed., Wiley-Interscience, 26–77.

Regnier, P., and Coauthors, 2013: Anthropogenic perturbation of the carbon fluxes from land to ocean. *Nat. Geosci.*, **6**, 597–607, https://doi.org/10.1038/ngeo1830.

Rodgers, K. B., J. Lin, and T. L. Frölicher, 2015: Emergence of multiple ocean ecosystem drivers in a large ensemble suite with an Earth system model. *Biogeosciences*, **12**, 3301–3320, https://doi.org/10.5194/bg-12-3301-2015.

Sánchez-García, L., J. E. Vonk, A. N. Charkin, D. Kosmach, O. V. Dudarev, I. P. Semiletov, and Ö. Gustafsson, 2014: Characterisation of three regimes of collapsing Arctic ice complex deposits on the SE Laptev sea coast using biomarkers and dual carbon isotopes. *Permafrost Periglacial Process.*, **25**, 172–183, https://doi.org/10.1002/ppp.1815.

Schlunegger, S., K. B. Rodgers, J. L. Sarmiento, T. L. Frölicher, J. P. Dunne, M. Ishii, and R. Slater, 2019: Emergence of anthropogenic signals in the ocean carbon cycle. *Nat. Climate Change*, **9**, 719–725, https://doi.org/10.1038/s41558-019-0553-2.

——, and Coauthors, 2020: Time of emergence and large ensemble intercomparison for ocean biogeochemical trends. *Global Biogeochem. Cycles*, **34**, e2019GB006453, https://doi.org/10.1029/2019GB006453.

Screen, J. A., and I. Simmonds, 2010: The central role of diminishing sea ice in recent Arctic temperature amplification. *Nature*, **464**, 1334–1337, https://doi.org/10.1038/nature09051.

Séférian, R., and Coauthors, 2019: Evaluation of CNRM Earth system model, CNRM-ESM2-1: Role of Earth system processes in present-day and future climate. *J. Adv. Model. Earth Syst.*, **11**, 4182–4227, https://doi.org/10.1029/2019MS001791.

Shindell, D. T., G. Faluvegi, D. M. Koch, G. A. Schmidt, N. Unger, and S. E. Bauer, 2009: Improved attribution of climate forcing to emissions. *Science*, **326**, 716–718, https://doi.org/10.1126/science.1174760.

Stedmon, C., R. M. W. Amon, A. Rinehart, and S. Walker, 2011: The supply and characteristics of colored dissolved organic matter (CDOM) to the Arctic Ocean. *Mar. Chem.*, **124**, 108–118, https://doi.org/10.1016/j.marchem.2010.12.007.

Stocker, B. D., and Coauthors, 2013: Multiple greenhouse-gas feedbacks from the land biosphere under future climate change scenarios. *Nat. Climate Change*, **3**, 666–672, https://doi.org/10.1038/nclimate1864.

Tank, S. E., M. Manizza, R. M. Holmes, J. W. McClelland, and B. J. Peterson, 2012: The processing and impact of dissolved riverine nitrogen in the Arctic Ocean. *Estuaries Coasts*, **35**, 401–415, https://doi.org/10.1007/s12237-011-9417-3.

Terhaar, J., J. C. Orr, C. Ethé, P. Regnier, and L. Bopp, 2019: Simulated Arctic Ocean response to doubling of riverine carbon and nutrient delivery. *Global Biogeochem. Cycles*, **33**, 1048–1070, https://doi.org/10.1029/2019GB006200.

——, R. Lauerwald, P. Regnier, N. Gruber, and L. Bopp, 2021: Around one third of current Arctic Ocean primary production

sustained by rivers and coastal erosion. *Nat. Commun.*, **12**, 169, https://doi.org/10.1038/s41467-020-20470-z.

Thibodeau, B., D. Bauch, and M. Voss, 2017: Nitrogen dynamic in Eurasian coastal Arctic ecosystem: Insight from nitrogen isotope. *Global Biogeochem. Cycles*, **31**, 836–849, https://doi.org/10.1002/2016GB005593.

Tietsche, S., D. Notz, J. H. Jungclaus, and J. Marotzke, 2011: Recovery mechanisms of Arctic summer sea ice. *Geophys. Res. Lett.*, **38**, L02707, https://doi.org/10.1029/2010GL045698.

Tremblay, J.-É., and J. Gagnon, 2009: The effects of irradiance and nutrient supply on the productivity of Arctic waters: A perspective on climate change. *Influence of Climate Change on the Changing Arctic and Sub-Arctic Conditions*, Springer, 73–93.

——, L. G. Anderson, P. Matrai, P. Coupel, S. Bélanger, C. Michel, and M. Reigstad, 2015: Global and regional drivers of nutrient supply, primary production and CO_2 drawdown in the changing Arctic Ocean. *Prog. Oceanogr.*, **139**, 171–196, https://doi.org/10.1016/j.pocean.2015.08.009.

Vancoppenolle, M., L. Bopp, G. Madec, J. Dunne, T. Ilyina, P. R. Halloran, and N. Steiner, 2013: Future Arctic Ocean primary productivity from CMIP5 simulations: Uncertain outcome, but consistent mechanisms. *Global Biogeochem. Cycles*, **27**, 605–619, https://doi.org/10.1002/gbc.20055.

van Drecht, G., A. F. Bouwman, J. M. Knoop, C. Meinardi, and A. Beusen, 2001: Global pollution of surface waters from point and nonpoint sources of nitrogen. *Sci. World J.*, **1**, 980756, https://doi.org/10.1100/tsw.2001.326.

Wassmann, P., and M. Reigstad, 2011: Future Arctic Ocean seasonal ice zones and implications for pelagic-benthic coupling. *Oceanography*, **24**, 220–231, https://doi.org/10.5670/oceanog.2011.74.

Wegner, C., and Coauthors, 2015: Variability in transport of terrigenous material on the shelves and the deep Arctic Ocean during the Holocene. *Polar Res.*, **34**, 24964, https://doi.org/10.3402/polar.v34.24964.

Winton, M., 2000: A reformulated three-layer sea ice model. *J. Atmos. Oceanic Technol.*, **17**, 525–531, https://doi.org/10.1175/1520-0426(2000)017<0525:ARTLSI>2.0.CO;2.